2006

Spectroscopy, production and decays of pentaquarks

Herry Kwee
College of William & Mary - Arts & Sciences

SPECTROSCOPY, PRODUCTION AND DECAYS OF PENTAQUARKS

A Dissertation

Presented to

The Faculty of the Department of Physics

The College of William and Mary in Virginia

In Partial Fulfillment

Of the Requirements for the Degree of

Doctor of Philosophy

---

by

Herry Kwee

2005

APPROVAL SHEET

This dissertation is submitted in partial fulfillment of

the requirements for the degree of

Doctor of Philosophy

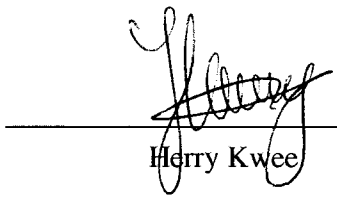

Herry Kwee

Approved by the Committee, August 2005

Christopher D. Carone, Chair

Carl E. Carlson

Keith Griffioen

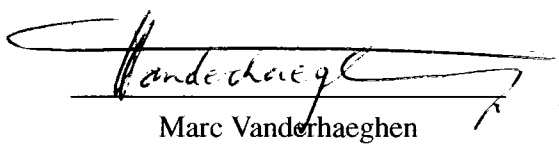

Marc Vanderhaeghen

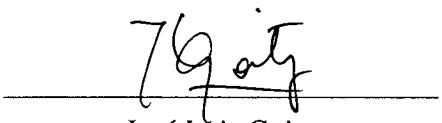

José Luis Goity
Hampton University

DEDICATION

I present this dissertation in honor of my beloved parents, Johnny and Heryawaty Kwee. You have been a great inspiration to me. I would not be where I am today without you.

TABLE OF CONTENTS

ACKNOWLEDGMENTS

I would like to express my deepest gratitude to my advisor Dr. Christopher Carone for his guidance and inspiration during my work in this dissertation and for all research collaborations that we did together and eventually become part of this dissertation. I would also like to express my gratitude to my other collaborators during my time as a graduate student in the physics department, Dr. Carlson, Dr. Vanderhaeghen, Dr. Nazaryan and Dr .Conroy. It has been a great pleasure to work with you all.

I would like to thank the other committee members, Dr. Griffieon and Dr. Goity for the time they took to read my thesis and to participate in the defense process. It has been a great experience. I would also like to take this chance to thank the physics department administrative staffs, Carol, Dianne, Paula and Sylvia and all the library staffs. I know that many things happen behind the scene more than I realize. You have done such a good job at making my time in the physics department sails through smoothly.

I would also like to take this opportunity to thank my brother Hendra, and my roommates Wirawan and Jong for all the support and prayer for me in the past few years. It has been a great blessing to live with you all. I also would like to thank my brother Yohanis which support me through prayer and periodic contact even though he is quite far away in Jakarta. I also can not finish this acknowledgment without including two families that have been a great part of my life in the past five years. First, I would like to express my deepest gratitude to Pastor Tom, his wife Cheryl and their children Gabrielle and Travis. Thank you very much for taking me to be part of your family. Your hospitality, prayer and support in the last five years have been indispensable. And the second family is Stan and Debbie Betz. Thank you for all your friendship, prayer and hospitality.

Finally special thanks to many friends that I have met in this country, Steve, Robert, Taylor, and Joey. Thank you for all the support and prayer over the last few years. It has been a great pleasure to know you all. Also I would like to thank a friend from my own country that I get to know much better after I came to this country, Agus Ananda. He has been a great friend and a good role model for me in my first year at William and Mary. Finally thank you to all friends that I do not have space to name one by one here, friends in the physics department, at my church, Grace Covenant, especially to Libby and Marion who came to my defense, and finally many thanks to friends in RUF, Crusade and Intervarsity, thank you all for your friendship and support.

LIST OF TABLES

LIST OF FIGURES

ABSTRACT

An extensive study of the production, decay and spectroscopy of pentaquarks has been done in this dissertation. At the time of this writing, the existence of the pentaquark has not been conclusively established. New experimental results for the pentaquark will come in the months ahead. A brief review of the current experimental status of the pentaquark is given in the Introduction. The pentaquark states are analyzed using the constituent quark model with the lowest-lying pentaquark multiplet shown to be an antidecuplet. The mass splittings within the antidecuplet emerge from spin-color and spin-flavor interactions between constituents and from hidden strangeness in the antidecuplet, rendering the nucleon-like states heavier than the S=1 Θ^+ state. In order to calculate such interactions, decompositions of the quark model color-flavor-spin-orbital wave functions must be obtained. A spin-1/2 state is assumed in this work. Assigning all quarks to the orbital ground state yields an odd parity state, while giving one quark a unit of orbital angular momentum leads to a state with even parity. Dominant spin-flavor interactions render certain parity-even pentaquark states lighter than states with all quarks in the spatial ground state. In this even-parity scenario, it is possible to explain the unusually narrow width of the Θ^+ by computing the overlap of this state with the kinematically allowed final states. The results are numerically small. Decays of other states within the antidecuplet are related to the Θ^+ by SU(3) symmetry and phase space. The photoproduction of the $\Theta^+(1540)$ resonance on the nucleon, through K and K^* Regge exchanges is also studied in this thesis. The size of the cross sections for the $\gamma n \to K^- \Theta^+$ and $\gamma p \to \bar{K}^0 \Theta^+$ reactions are compared and their sensitivity to the spin-parity assignments $J^P = \frac{1}{2}^{\pm}, \frac{3}{2}^{\pm}$ for the Θ^+ resonance is investigated. This model allows us to estimate the cross sections corresponding to a given upper bound on the Θ^+ width. The cross sections on the neutron are found to be around a factor 5 larger than the ones on the proton, due to the presence of charged Kaon exchange. Furthermore, the photon asymmetry is found to display a pronounced sensitivity to the parity of the Θ^+, making it a promising observable for determining the spin and parity of the Θ^+ resonance.

SPECTROSCOPY, PRODUCTION AND DECAYS OF PENTAQUARKS

CHAPTER 1

Introduction

In January 2003, SPring-8 published the first claim of experimental evidence for an $S = 1$ baryon resonance with a mass of 1540 MeV and a narrow decay width [1]. This state, known as the Θ^+ today, cannot be a 3-quark baryon. It is natural to interpret it as a pentaquark state, that is, as a state made from four quarks and one antiquark, $q^4\bar{q}$. Within the same year a great number of experiments confirmed the observation of the Θ^+ [2, 3, 4, 5, 6, 7, 8, 9, 10]. These experiments represent a great variety of production and detection methods. We will spend some time discussing the most important of these experiments to better understand the significance of the Θ^+ resonance claim. We will demonstrate that even though some of the claims for the observation of a pentaquark state have been challenged, there is still significant evidence otherwise, rendering the pentaquark issue unresolved for the moment. The first experiment by the LEPS collaboration [1] involves a photoproduction process on carbon nuclei. The solid histograms in Fig 1.1 show the missing mass (corrected for Fermi motion) of each kaon in the $\gamma C \rightarrow K^+K^-X$ reaction, while the dashed histograms show events where a recoil proton was detected. In this reaction, the photon can hit either a proton or a neutron and the Fermi motion correction is used to estimate the momentum of the nucleon hit by the photon. In the reactions

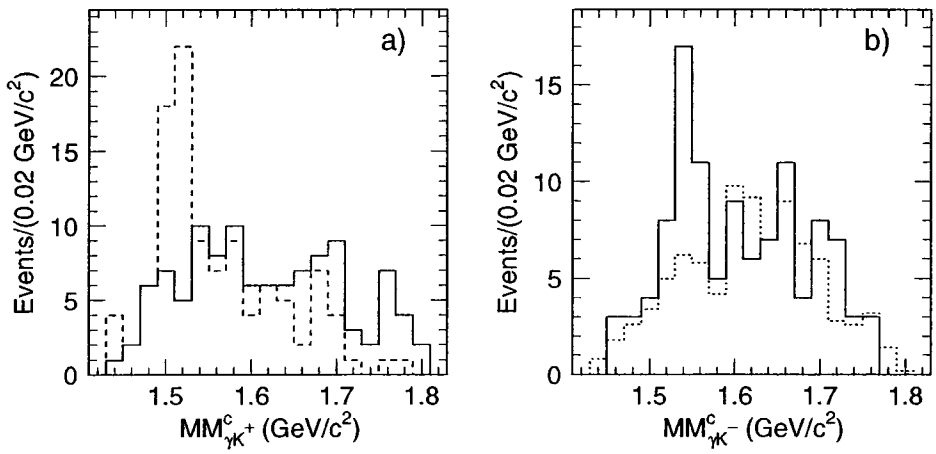

FIG. 1.1: K^+ and K^- missing mass spectra (corrected for Fermi motion) for the reaction $\gamma C \rightarrow K^+K^-X$ in Spring-8 experiment [1]. The solid histogram shows events where no proton was detected. The $\Lambda(1520)$ resonance is seen on the left in the dashed histogram, where a coincident proton was detected. Possible evidence for the Θ^+ is seen as the peak on the right.

where the photon hits a proton, such as the $\gamma p \rightarrow K^+\Lambda^*(1520)$ followed by the decay $\Lambda^* \rightarrow pK^-$, an energetic recoil proton is often detected in the reactions. The peak seen on the left dashed histogram is the $\Lambda(1520)$ resonance. If the photon hits a neutron such as in $\gamma n \rightarrow K^-\Theta^+$ followed by the decay $\Theta^+ \rightarrow nK^+$, the energetic proton will be missing. The peak on the right solid histogram was the one interpreted as the Θ^+ resonance. Spring 8 detector (LEPS) has a forward-angle-only acceptance and is symmetric for detection of positive and negative particles which is helpful in comparing the $\Lambda(1520)$ and Θ^+ peaks.

There are several criticisms of this experiment. First, the signal consists of only 19 counts in the peak on the top of 17 counts background, very low statistics indeed. Second, the Fermi motion correction used to analyze the data is an empirical correction, an approximation which is good only if the momentum transfer to the residual nucleus is small. Finally, the background estimate is not well determined. The statistical significance of the

signal is obtained by using the background from quasi-free production of kaon pairs off either a proton or neutron (the dashed histogram). It is not clear if this is the dominant background process.

The next several experiments we will discuss searched for the Θ^+ in photoproduction off a nucleon. These include the CLAS result for the reaction $\gamma d \rightarrow K^+K^-p(n)$ [2], the SAPHIR result for $\gamma p \rightarrow K^0_s K^+ n$ [3], and the CLAS result for $\gamma p \rightarrow \pi K^+ K^- n$ [4]. In the first CLAS experiment [2], the neutron is not detected directly but deduced from the missing four-momentum, with very low background (< 15 under the neutron peak in Fig. 1.2). The proton can only be detected if it has momentum well above its Fermi momentum (> 300 MeV/c), requiring it to be more than just a spectator in the reaction. There must be some mechanism, such as rescattering of the K^- from the proton, that will give the proton higher momentum. It has been shown that K^- rescattering happens at about 30-50% probability for $\Lambda(1520)$ production [11]. As a consequence of this required additional mechanism, the shape of background estimate becomes difficult. The statistical significance of this experiment for the Gaussian shape background in Fig. 1.2 is 5.2σ. The alternative background shape in Fig. 1.2 will give a 3σ statistical significance. There is a possibility of kinematic reflections [12] contributing to the background even though that possibility has been challenged because it violates charge conjugation conservation [13].

The reaction $\gamma p \rightarrow K^0_s K^+ n$ studied by the SAPHIR collaboration was the first exclusive reaction that does not require any rescattering or nuclear effects [3]. The mass spectrum, after an angle cut on the K^0 has been applied (center-of-mass angle with $\cos\theta_{K^0} > 0.5$, requiring it to be only at forward angles), is shown in Fig. 1.3 and has a statistical significance of around 4σ. The SAPHIR result predicts a large cross section which contradicts the result of the CLAS measurement on the same reaction. It also has been ruled out by a new high-statistics result from the CLAS collaboration [14]. The new result from CLAS shows a flat mass spectrum regardless of the K^0 angle. This seems to be consistent with most production calculations which show that the Θ^+ production cross

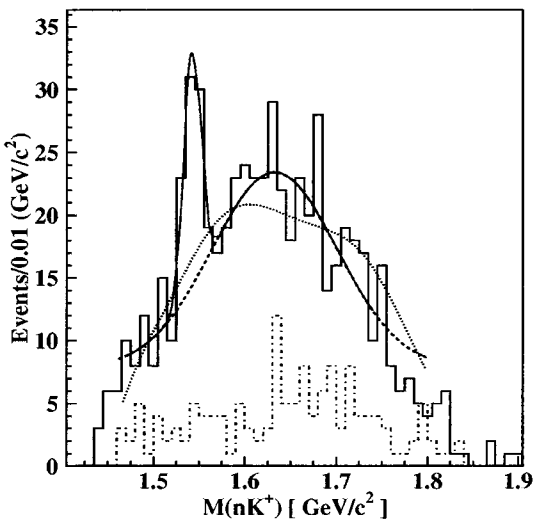

FIG. 1.2: Data from CLAS [2] for the reaction $\gamma d \rightarrow K^+K^-p(n)$. The missing mass of the K^-p system, which is the same as the mass of the nK^+ system, is shown along with two estimates of the background shape (smooth curves). The contribution of the $\Lambda(1520)$ events, which were cut out, are shown by the dashed histogram at the bottom.

sections on proton targets are significantly suppressed compared to those on neutron targets [15, 16, 17, 18].

The original CLAS result on a proton target provided some of the best evidence for the existence of the Θ^+ [4]. The exclusive reaction, $\gamma p \rightarrow \pi^+K^-K^+n$ is very clean, there is no ambiguity due to rescattering from other nucleons, and the strangeness of the final state is known. The final result is shown in Fig. 1.4, where cuts have been applied on the π^+ angle ($\cos\theta_\pi > 0.8$) and K^+ angle ($\cos\theta_{K^+} > 0.6$) in the center-of-mass frame. The cuts for this analysis were chosen by the experimenters to specifically remove the dominant background process, vector meson production reactions, with the assumption that the Θ^+ can be produced through an s-channel diagram [4]. The mass peak from this experiment is at 1.55 ± 0.01 GeV, which is 0.01 GeV higher than the average mass from other experiments. The mass peak has a statistical significance in excess of 7σ, but a more realistic estimate is probably 4σ [11]. This experiment can be criticized on two

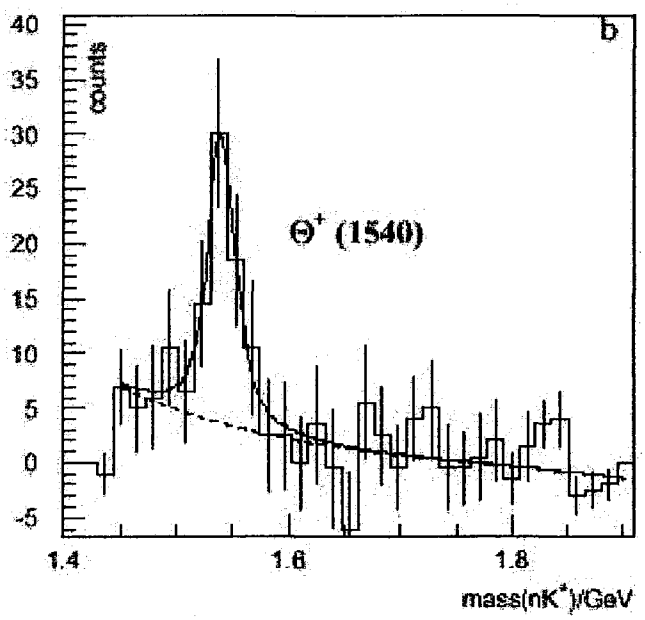

FIG. 1.3: The mass of the nK^+ system for the reaction $\gamma p \to K^+ K_s^0(n)$ from SAPHIR [3].

points. The first is that justification for the angle cuts comes from assumptions about the production mechanism and the dominant background process. Whether these assumptions are correct remains an open question. Second, the mass peak at 1.55 ± 0.01 GeV is inconsistent with other experiments, bringing into question the interpretation of the peak as the Θ^+. Also, as for the SAPHIR case, it has been shown by many calculations that the Θ^+ production cross sections on the proton targets are significantly suppressed compared to those on neutron targets [15, 16, 17, 18].

The next experiment we discuss, the DIANA experiment, uses kaon beams to produce the Θ^+ [5]. The reaction is $K^+\mathrm{Xe} \to K^0 p \mathrm{Xe}'$, followed by the decay $K^0 \to \pi^+\pi^-$. The final-state $p\pi^+\pi^-$ particles are detected by ionization tracks in the Xe bubble chamber photographs. Since the particle identification is based on the kinematics of the two-body K^0 decay to $\pi^+\pi^-$, there is little chance of particle misidentification. Also the hadronic

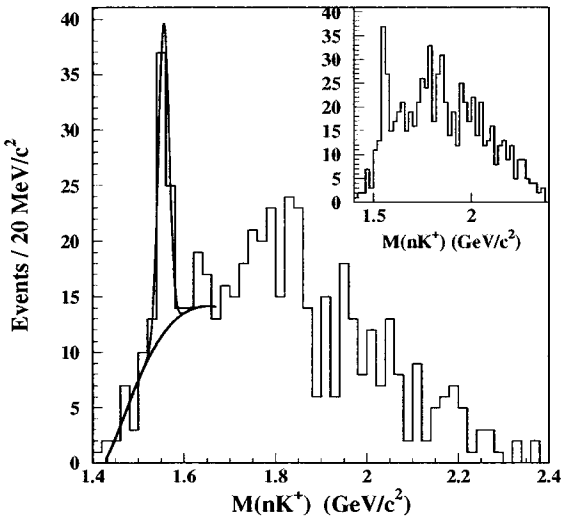

FIG. 1.4: Data from CLAS [4] on a proton target for the reaction $\gamma p \rightarrow \pi^+ K^+ K^- (n)$ after cuts on the K^+ and π^+ angles. The inset shows the data when only the $\cos\theta_\pi > 0.8$ cut has been applied. The curve is a fit to the peak and a smooth background estimated from partial wave analysis of the uncut data.

reaction mechanism conserves strangeness and the initial state has the same quantum numbers as the Θ^+. The final data sample after the cuts on the proton and K^0 emission angles (both are required to be $< 100°$ in the lab frame and their azimuthal angles must be at least $90°$ apart to remove rescattering events) is shown in Fig. 1.5. The mass spectrum is calculated from the invariant mass of the pK^0 system. The background estimate, shown in the Fig. 1.5 as the dashed histogram is obtained from a "mixed event" technique, where the protons and K^0 are combined randomly from different events. Statistical significance of this experiment is around 4.4σ. The first thing one can notice from Fig. 1.5 is the low statistics. The peak is localized within a single bin where there are only about 20 events on top of 20 background events. Also without the emission angle cuts it is hard to see the peak. Details on the sensitivity of the mass spectrum to the angle cuts were not provided, nor were details of the modeling of the kaon charge-exchange for the background

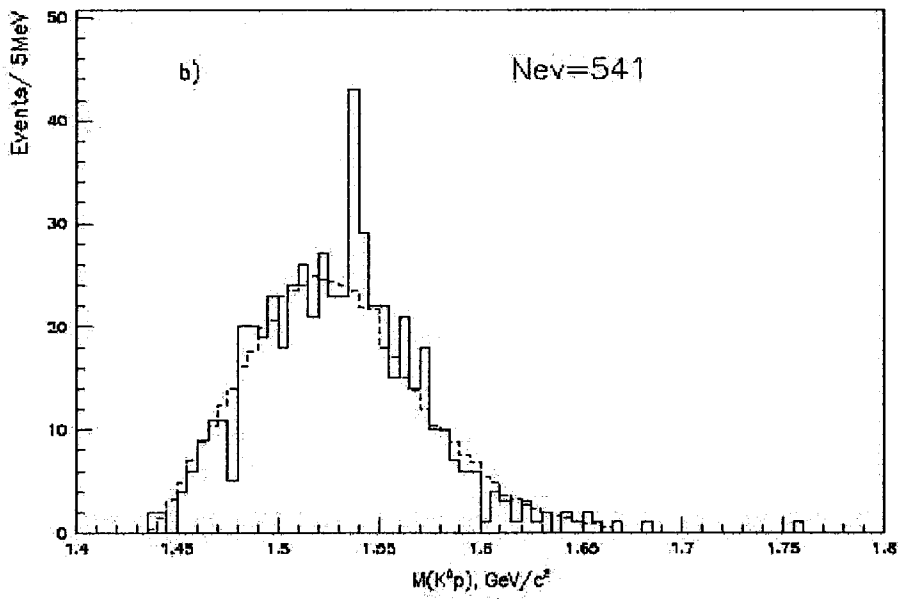

FIG. 1.5: The invariant mass of the pK^0 system after analysis cuts for the reaction $K^+Xe \rightarrow pK^0_sXe'$ from DIANA [5]. The dotted histogram is from a mixed-event technique expected to represent the background.

estimate.

The next group of experiments to which we will turn our attention is the electroproduction of the Θ^+ on the nucleon [7, 8]. The first of such experiments, the HERMES experiment, measured the reaction $e^+d \rightarrow pK^0X$ using the DESY positron beam at 27.6 GeV on a stationary deuterium target [7]. The final result shows a peak at 1528 MeV for the $\pi^+\pi^-p$ invariant mass spectrum. The K^0, reconstructed from the $\pi^+\pi^-$ invariant mass spectrum, has a clear peak. This result has a statistical significance of $3.4-4.3\sigma$ [7], but also has several weaknesses. First of all, the resonance mass peak is at 1528 MeV, about 10 MeV below the results from other experiments. The other issue is the strangeness tag. Unlike DIANA, the HERMES experiment can not differentiate between the possibilities that the peak is a Θ^+ or a new Σ^{*+}. This tagging issue and the shifted peak mentioned above make the interpretation as the Θ^+ problematic.

The Zeus experiment measured the similar reaction $e^+p \rightarrow pK^0X$, also at DESY, at

a center-of-mass energy of about 300 GeV [8]. At such high energy, hadrons are thought to be produced mainly through fragmentation processes. Fragmentation proceeds via "string-breaking", where one quark absorbs almost all of the momentum transfer from the scattered lepton and breaks away from the residual diquark after breaking all the color-force flux-tubes that connect them. As will be discussed later in this introduction, this process is thought to be unlikely to produce the Θ^+. ZEUS result shows a clear peak at 1522 MeV after a cut on the momentum transfer of $Q^2 > 20$ GeV^2. At $Q^2 > 1$ GeV^2, no clear peak is visible. This raises doubts as to whether ZEUS did actually see the Θ^+ resonance.

Next we will discuss the Θ^+ production from hadron beam experiments, the COSY-TOF experiment [6] and the SVD experiment [9]. The COSY-TOF experiment [6] measured the exclusive hadron reaction $pp \rightarrow \Sigma^+ K^0_s p$ using a 2.95 GeV/c proton beam on a liquid hydrogen target. The strangeness is tagged by the Σ^+. Particle identification is done entirely by geometric reconstruction. This is very accurate for near-threshold reactions. The result is a peak at 1.53 GeV with a statistical significance of 4 to 5σ, depending on the background shape. The experiment has good statistics. The only problem with this experiment is the broad hump near threshold that is maximum at 1.47 GeV and that is unexplained (see Fig. 1.6). The actual shape of the hump affects the number of background events under the peak. More data in the future is needed to solve this problem. The COSY-TOF collaboration did take additional data in November 2004 which was expected to increase their statistics by a factor of 5 [19]. The new run used a slightly higher beam energy so that the peak will not be very close to the end point. Currently, data analysis is being performed and we can expect their result in the near future.

The SVD collaboration measured $pA \rightarrow pK^0X$, where A represents either C, Si or Pb using the 70 GeV proton beam at the IHEP accelerator in Russia [9]. Their final result for the pK^0 system invariant mass is obtained using only 5 charged tracks. There is also a 90° forward in center-of-mass angle cut on the pK^0 system. The result is a peak

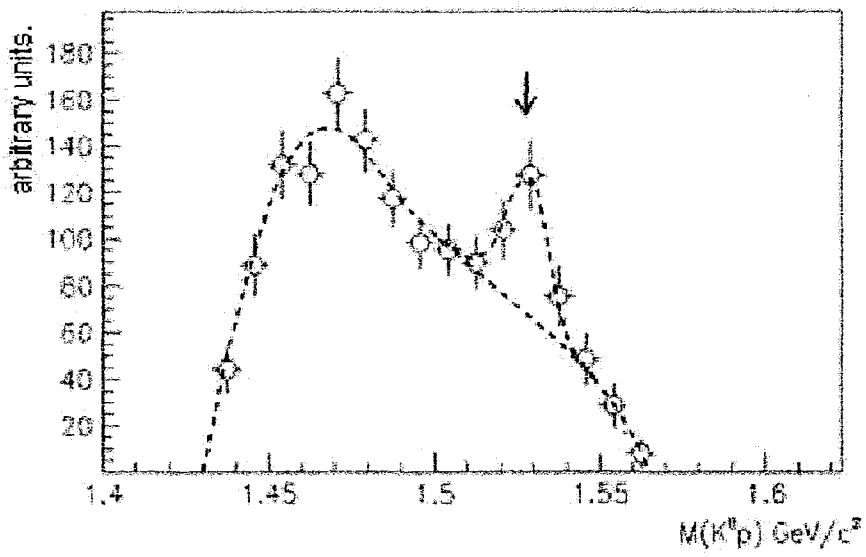

FIG. 1.6: The invariant mass of the K^0p system after acceptance corrections from COSY-TOF [6] for the reaction $pp \rightarrow \Sigma^+ K^0_s p$ at near-threshold energies.

at 1526 MeV with around 3σ statistical significance. The low statistics as well as the shifted mass and the additional angle cuts render this experimental claim for the Θ^+ not convincing.

The final group of experiments we discuss produce the Θ^+ using neutrino beams [10]. The ITEP group analyze a collection of 5 neutrino experiments from bubble chamber using the $\nu A \rightarrow pK^0X$ reaction, where A represents either hydrogen (H), deuterium (D) or neon (Ne). Most of their data is obtained from the Ne target, since the statistics for the other two targets are very low. The advantage of this experiment is the background. The background estimate is done by taking random combinations of protons from one event and K^0's from another event. The two must be uncorrelated and give rise to a smooth background. The result is a low background. The disadvantages include an inability to determine the K^0 strangeness and the low statistics. The experiment only measures a peak of 20 counts above a background of 12 counts. The final result is a peak at 1533 MeV with around 3.5σ statistical significance.

There are also a fairly large number of experiments [20, 21, 22, 23, 24, 25, 26, 27, 28, 29, 30] that did not find any evidence for the Θ^+. Most of these experiments are high energy-high statistics experiments and they fall into two categories. The first category includes the e^+e^- experiments, BES [20], BaBar [21], Belle [22], and the LEP experiment [23]. The second category is the hadron beam experiments, including HERA-B [24], SPHINX [25], HyperCP [26], and the CDF experiment [27].

The e^+e^- experiments do not present a credible challenge to the existence of the Θ^+ since it is very difficult to produce the Θ^+ in this way. In order to produce the Θ^+ in e^+e^- collisions, at least 5 quarks and 5 antiquarks must be produced. Even though this number is typical in such facilities, to have 4 quarks and an antiquark localized in space with very small relative velocity to form a Θ^+ state is highly unlikely. Since it is difficult to detect a neutron most of the e^+e^- experiments look for a resonance in the pK^0 invariant mass. The result usually is a mass spectrum without any structure. This negative result actually casts doubt on the validity of these Θ^+ searches since the known Σ^*+ resonances should be seen in these experiments (such as the $\Sigma(1670)$ with an estimated width of 60 MeV) but are not.

The hadron beam experiments present a more serious concern. Since these experiments have more quarks (antiquarks) in the initial state, we would expect that the pentaquark states will be easier to produce. However, as mentioned above when we discussed the ZEUS result, at this energy range most hadrons are thought to be produced by fragmentation process, which make the production of the pentaquark state unlikely. The indication that hadrons are unlikely to be produced with these kind of experiments are the absence of any known Σ^*+ resonance in the pK^0 mass spectra.

Each of the experiments we have discussed that claim a signal for the Θ^+ have some weaknesses that make such claim subject to dispute. However, taken together, it is hard to imagine that the Θ^+ is just an artifact. As we have seen, null results from higher energy experiments are also ambiguous. These experiments do not have the optimal production

mechanisms for the creation of pentaquark states. Thus at the time of this writing the debate over the existence of the Θ^+ remains unresolved. Understanding the properties of the Θ^+ from the underlying theory of the strong interaction is therefore of the utmost importance. This is the focus of this thesis.

In the next 3 chapters of this work we will study the Θ^+ and other related pentaquark states from the constituent quark model point of view . In Chapter 2, we study the properties of the pentaquark by assigning all the quarks and antiquark to the ground state in a naive quark model. In this model, the Θ^+ and the other members of the same multiplet have negative parity. We also study the mass spectrum of this multiplet. In Chapter 3, we assign one of the quarks one unit of angular momentum. It has been shown in Ref. [31] that this configuration can be lighter than the negative parity case. In Chapter 4, we explore a scenario that explains the narrow width Θ^+ in a constituent quark model. Finally we close in Chapter 5 with a calculation of Θ^+ photoproduction in a Regge model and its decay angular distribution with the hope that future higher statistics experiments will resolve the pentaquark issue.

CHAPTER 2

Phenomenology of the Pentaquark Antidecuplet

2.1 Introduction

In this chapter, we study consequences of describing the Θ^+ within the context of conventional constituent quarks models, in more focused detail than was done in earlier work [32, 33, 34, 35] and with new results. In these models, all quarks are in the same spatial wave function, and spin dependent mass splittings come from either color-spin or flavor-spin exchange. The Θ^+ made this way has negative parity. We treat it as a flavor antidecuplet, with spin-1/2 because this state has, at least by elementary estimates, the lowest mass by a few hundred MeV among the Θ^+'s that can be made with all quarks in the ground spatial state.

The pentaquark by now has some history of theoretical study. In the context of constituent quark models, it was analyzed relatively early on [32, 33, 34, 35], but the subject was not pursued, probably for lack of experimental motivation. (The first of [32, 33] gives a simple estimate of the Θ^+ mass of 1615 MeV and then states "There definitely

is no $Z^*(I = 0)$ state at such a low mass.") Much of the effort shifted to studying pentaquarks involving charmed as well as strange quarks [36, 37, 38], before the recent flurry of theoretical attention [31, 39, 40, 41, 42, 43, 44, 45, 46, 47, 48].

Pentaquarks have also been studied in the context of the Skyrme model [49, 50, 51]. Ref. [51] in particular makes a striking prediction, based on the assumption that the Θ^+ is a member of a flavor antidecuplet and that the nucleon-like members of this decuplet are the observed $N^*(1710)$ states, that the Θ^+ would have a mass of about 1530 MeV and a width less than 15 MeV. Note that in this case the Θ^+ is a positive parity state.

We may elaborate on the Θ^+ states and masses in quark models briefly before proceeding. In outline, there are several ways to make a Θ^+, and one can obtain Θ^+'s which are isospin 0, 1, or 2. The mass splittings between the states can be estimated using, say, the color-spin interactions described in more detail in the next section. Techniques and useful information may be found in [32, 33, 38, 52]. The lightest Θ^+ state is the isosinglet (in the $\overline{10}$) with spin-1/2. The isosinglet spin-3/2 is a few hundred MeV heavier. The heaviest states are the isotensor spin-1/2 and (somewhat lighter) spin-3/2 states. The mass gap between the lightest and heaviest of the Θ^+'s is triple the mass gap between the nucleon and the $\Delta(1232)$, if one does not account for changes in the quarks's spatial wave functions (*e.g.*, due to changes in the Bag radius), or the better part of a GeV. The isovector masses lie in between the two limits. These statements are considered in quantitative detail in Ref. [53]

In the next section, we will discuss the color-flavor-spin wave functions of the antidecuplet that contains the Θ^+. This is a necessary prelude to a discussion of the mass splittings and decays of the full decuplet, which follows in Section III. One intriguing result is the roughly equal mass spacing of the antidecuplet, with the Θ^+ lightest. Normally one expects the strange state to be heavier that the non-strange one. The explanation of this counterintuitive behavior is hidden strangeness, that is, there is a fairly high probability of finding an $s\bar{s}$ pair in the non-strange state. We also show that there is a markedly

different pattern of kinematically allowed decays, depending of whether spin-isospin or spin-color exchange interactions are relevant in determining the mass spectrum. We close in Section IV with some discussion.

2.2 Wave Function

There are two useful ways to compose the pentaquark state. One is to build the q^4 state from two pairs of quarks and then combine with the $\bar{q}$. The other is to combine a q^3 state with a $q\bar{q}$ to form the pentaquark. We first represent the pentaquark state in terms of states labelled by the quantum numbers of the first and second quark pairs. Since the antiquark is always in a ($\bar{\mathbf{3}}$,$\bar{\mathbf{3}}$,1/2) (color,flavor,spin) state, we know immediately that the remaining four-quark (q^4) state must be a color $\mathbf{3}$. The flavor of a generic q^4 state can be either a $\mathbf{3}$, $\bar{\mathbf{6}}$, $\mathbf{15}_M$, or $\mathbf{15}_S$ (where S and M refer to symmetry and mixed symmetry under quark interchange, respectively). However, only the $\bar{\mathbf{6}}$ can combine with the $\bar{\mathbf{3}}$ antiquark to yield an antidecuplet. Finally, the spin of the q^4 state can be either 0 or 1 if the total spin of the state is 1/2. However, it is not difficult to show that any state constructed with the correct quantum numbers using the spin-zero q^4 wave function will be antisymmetric under the combined interchange of the two quarks in the first pair with the two quarks in second pair; this is inconsistent with the requirement that the four-quark state be totally antisymmetric. Thus we are led to the unique choice

$$|(C,F,S)\rangle_{q^4} = |(\mathbf{3},\bar{\mathbf{6}},1)\rangle \ . \tag{2.1}$$

Figure 2.1 shows the possible quark pair combinations that can provide a $(\mathbf{3},\bar{\mathbf{6}},1)$ four-quark state. The symmetry under interchange of quarks 1 and 2, or 3 and 4 is immediate from each of the Young's Tableau shown. The symmetry under interchange of the first and second quark pairs is indicated in brackets next to the tableau. Only three combinations have the right symmetry under quark interchange to form a totally antisymmetric q^4 state,

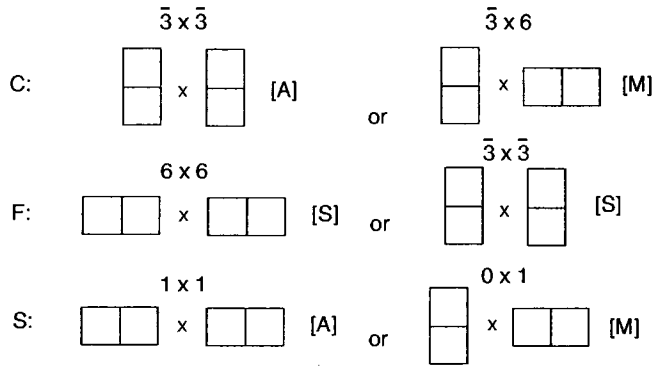

FIG. 2.1: Quark pair states that can be appropriately combined to yield a total (C,F,S) state $(\mathbf{3},\bar{\mathbf{6}},1)$.

namely

$$|(\bar{\mathbf{3}},\mathbf{6},1)(\bar{\mathbf{3}},\mathbf{6},1)\rangle \ , \ \frac{1}{\sqrt{2}}\left(|(\mathbf{6},\mathbf{6},0)(\bar{\mathbf{3}},\mathbf{6},1)\rangle + |(\bar{\mathbf{3}},\mathbf{6},1)(\mathbf{6},\mathbf{6},0)\rangle\right) \ ,$$

$$\frac{1}{\sqrt{2}}\left(|(\mathbf{6},\bar{\mathbf{3}},1)(\bar{\mathbf{3}},\bar{\mathbf{3}},0)\rangle + |(\bar{\mathbf{3}},\bar{\mathbf{3}},0)(\mathbf{6},\bar{\mathbf{3}},1)\rangle\right) \ .$$

The requirement of total antisymmetry of the q^4 wave function, determines the relative coefficients. We find that the properly normalized state is given by

$$\begin{aligned} |(1,\overline{\mathbf{10}},1/2)\rangle \ &= \ \frac{1}{\sqrt{3}}|(\bar{\mathbf{3}},\mathbf{6},1)(\bar{\mathbf{3}},\mathbf{6},1)\rangle + \frac{1}{\sqrt{12}}\left(|(\mathbf{6},\mathbf{6},0)(\bar{\mathbf{3}},\mathbf{6},1)\rangle + |(\bar{\mathbf{3}},\mathbf{6},1)(\mathbf{6},\mathbf{6},0)\rangle\right) \\ &- \ \frac{1}{2}\left(|(\mathbf{6},\bar{\mathbf{3}},1)(\bar{\mathbf{3}},\bar{\mathbf{3}},0)\rangle + |(\bar{\mathbf{3}},\bar{\mathbf{3}},0)(\mathbf{6},\bar{\mathbf{3}},1)\rangle\right) \ , \end{aligned} \tag{2.2}$$

where we have suppressed the quantum numbers of the antiquark, ($\bar{\mathbf{3}}$,$\bar{\mathbf{3}}$,1/2), which are the same in each term. Also tacit on the right-hand side is that each q^4 state is combined to $(\mathbf{3},\bar{\mathbf{6}},1)$. The signs shown in Eq. (2.2) depend on sign conventions for the states on the right-hand side. For the Θ^+ component,spin $\uparrow$, we find

$$\begin{aligned} |(\bar{\mathbf{3}},\mathbf{6},1)(\bar{\mathbf{3}},\mathbf{6},1)\rangle \ &= \ \frac{1}{24\sqrt{3}}(c_1^j c_2^k - c_1^k c_2^j)c_3^m c_4^n \bar{c}_k \epsilon_{jmn} \\ &\times \ [(2uudd + 2dduu - udud - uddu - duud - dudu)\bar{s}] \\ &\times \ [\{\uparrow\uparrow(\uparrow\downarrow + \downarrow\uparrow) - (\uparrow\downarrow + \downarrow\uparrow)\uparrow\uparrow\}\downarrow - (\uparrow\uparrow\downarrow\downarrow - \downarrow\downarrow\uparrow\uparrow)\uparrow] \ , \end{aligned}$$

(2.3)

$$|(\mathbf{6},\mathbf{6},0)(\bar{\mathbf{3}},\mathbf{6},1)\rangle = \frac{1}{24\sqrt{3}}(c_1^j c_2^k + c_1^k c_2^j)c_3^m c_4^n \bar{c}_k \epsilon_{jmn} \times [(2uudd + 2dduu - udud - uddu - duud - dudu)\bar{s}] \times [(\uparrow\downarrow - \downarrow\uparrow)\uparrow\uparrow\downarrow - \frac{1}{2}(\uparrow\downarrow - \downarrow\uparrow)(\uparrow\downarrow + \downarrow\uparrow)\uparrow] , \quad (2.4)$$

$$|(\mathbf{6},\bar{\mathbf{3}},1)(\bar{\mathbf{3}},\bar{\mathbf{3}},0)\rangle = \frac{1}{24}(c_1^j c_2^k + c_1^k c_2^j)c_3^m c_4^n \bar{c}_k \epsilon_{jmn}[(ud - du)(ud - du)\bar{s}] \times [\uparrow\uparrow(\uparrow\downarrow - \downarrow\uparrow)\downarrow - \frac{1}{2}(\uparrow\downarrow + \downarrow\uparrow)(\uparrow\downarrow - \downarrow\uparrow)\uparrow] . \quad (2.5)$$

Here we have written the color wave function in tensor notation for compactness, with $c^i \equiv (r, g, b)$. The remaining component states in Eq. (2.2) can be obtained from Eqs. (2.4) and (2.5) by exchanging the first and second pair of quarks. With these results, one may construct other antidecuplet wave functions by application of SU(3) and isospin raising and lowering operators.

It is often convenient for calculational purposes to have a decomposition of the pentaquark wave function in terms of the quantum numbers of the first three quarks, and of the remaining quark-antiquark pair. The quark-antiquark pair can be either in a 1 or 8 of color, which implies that we must have the same representations for the three-quark (q^3) system, in order that a singlet may be formed. As for flavor, the q^3 and $q\bar{q}$ systems must both be in 8's: the $q\bar{q}$ pair cannot be in a flavor singlet, since there is no way to construct a $\overline{10}$ from the remaining three quarks, and the q^3 state must be an 8 since the remaining possibilities (1 and 10) do not yield an antidecuplet when combined with the $q\bar{q}$ flavor octet. Finally, the $q\bar{q}$ spin can be either 0 or 1, which implies that the q^3 spin can be either $1/2$ or $3/2$. The states consistent with q^3 antisymmetry are then

$$|(1,8,1/2)(1,8,0)\rangle \ , \ |(1,8,1/2)(1,8,1)\rangle \ , \ |(8,8,3/2)(8,8,1)\rangle \ ,$$
$$|(8,8,1/2)(8,8,0)\rangle \ , \ |(8,8,1/2)(8,8,1)\rangle$$

Again, we may find the coefficients by requiring that the total wave function is antisymmetric under interchange of the four quarks. Alternatively, we may take the overlap of

any of these states with the wave function that we have already derived in Eqs. (2.2)-(2.5). The details and explicit results will be presented in a longer publication [53]. We find

$$\begin{aligned} |(1,\overline{10},1/2)\rangle &= \frac{1}{2}|(1,8,1/2)(1,8,0)\rangle + \frac{\sqrt{3}}{6}|(1,8,1/2)(1,8,1)\rangle \\ &- \frac{\sqrt{3}}{3}|(8,8,3/2)(8,8,1)\rangle + \frac{1}{2}|(8,8,1/2)(8,8,0)\rangle \\ &+ \frac{\sqrt{3}}{6}|(8,8,1/2)(8,8,1)\rangle \ . \end{aligned} \tag{2.6}$$

Our sign conventions may be summarized by noting that each state on the right-hand side of Eq. (2.6) contains the term $uudd\bar{s}\uparrow\uparrow\downarrow\uparrow\downarrow\ rbgr\bar{r}$ with positive coefficient.

Two interesting observations can be made at this point. First, Eqs. (2.2)-(2.5) allow us to compute the expectation value of $S_h = \sum_i |S_i|$, where S_i is the strangeness of the i^{th} constituent. This gives us the average number of quarks in the state with either strangeness $+1$ or -1. For the Θ^+ state, the result is obviously 1; Using the SU(3) raising operator that changes $d \rightarrow s$ and $\bar{s} \rightarrow -\bar{d}$, it is straightforward to evaluate the same quantity for members of the antidecuplet with smaller total strangeness. We find

$$\langle\Theta^+|S_h|\Theta^+\rangle = 3/3\ ,\ \langle N_5|S_h|N_5\rangle = 4/3\ ,\ \langle\Sigma_5|S_h|\Sigma_5\rangle = 5/3\ ,\ \langle\Xi_5|S_h|\Xi_5\rangle = 6/3\ , \tag{2.7}$$

where N_5, Σ_5 and Ξ_5 represent the strangeness $0,-1$ and -2 members of the $\overline{10}$, respectively. The nonstrange member of the $\overline{10}$ is heavier than the Θ^+ because it has, on average, $m_s/3$ more mass from its constituent strange and antistrange quarks.

We also note that our decomposition in Eq. (2.6) allows us to easily compute overlaps with states composed of physical octet baryons and mesons. For example, the first term in Eq. (2.6) may be decomposed for the Θ^+

$$|(1,8,1/2)(1,8,0)\rangle = \frac{1}{\sqrt{2}}(pK^0 - nK^+)\ . \tag{2.8}$$

The sizes of the coefficients of these terms affect the rate of the "break-apart" decay modes, such as $\Theta^+ \rightarrow NK^+$. We therefore find that the smallness of the observed Θ^+

decay width ($\leq$ 21 MeV) does not originate with small group theoretic factors in the quark model wave function.

2.3 Antidecuplet Masses and Decays

Using the observed mass and width of the Θ^+, one may make predictions for the decay widths of other members of the antidecuplet. Here we consider the decays $\overline{10} \rightarrow BM$ where B (M) is a ground state octet baryon (meson). We assume exact SU(3)$_F$ symmetry in the decay amplitudes, but take into account SU(3)$_F$ breaking in the mass spectra. Mass splittings within the antidecuplet obey an equal spacing rule when the strange quark mass is the only source of SU(3)$_F$ breaking. We compute these splittings within the framework of the MIT bag model [54, 55], using the original version for the sake of definiteness, including effects of single gluon exchange interactions between the constituents. (See also [56, 57]; these works show how the overall mass level of a multiquark or gluonic state may be shifted, with only small changes in the predictions for ground state baryons and for spin-dependent splittings.) We also consider the possibility of dominant spin-isospin constituent interactions, which would be expected if nonstrange pseudoscalar meson exchange effects are important [58]. The predicted spectra differ significantly and yield distinguishable patterns of kinematically accessible decays.

In the bag model, the mass of a hadronic state is given by

$$M = \frac{1}{R}\left\{\sum \Omega_i - Z_0 + \alpha_s C_I\right\} + B\frac{4\pi R^3}{3} \tag{2.9}$$

where Ω_i/R is the relativistic energy of the i^{th} constituent in a bag of radius R,

$$\Omega = (x^2 + m^2R^2)^{1/2} \ , \tag{2.10}$$

and x is a root of

$$\tan x = \frac{x}{1 - mR - \Omega} \ . \tag{2.11}$$

The parameter Z_0 is a zero-point energy correction, and B is the bag energy per unit volume. In the conventional bag model, $Z_0 = 1.84$ and $B^{1/4} = 0.145$ GeV. The term $\alpha_s C_I$ represents the possible interactions among the constituents. We first take into account the color-spin interaction originating from single gluon exchange, so that

$$\alpha_s C_I = -\frac{\alpha_s}{4}\langle 1,\overline{10},1/2|\sum_{i<j}\mu(m_i,m_j)\,\lambda_i\cdot\lambda_j\,\sigma_i\cdot\sigma_j\,|1,\overline{10},1/2\rangle \tag{2.12}$$

where $\alpha_s = 2.2$ is the value of the strong coupling appropriate to the bag model, and $\mu(m_i,m_j)$ is a numerical coefficient that depends on the masses of the of the i^{th} and j^{th} quarks. For the case of two massless quarks, $\mu(0,0) \approx 0.177$; the analytic expression for arbitrary masses can be found in Ref. [55].

We take into account the effect of SU(3) breaking (*i.e.*, the strange quark mass) in both Ω_i and in the coefficients $\mu(m_i,m_j)$. To simplify the analysis, we break the sum in Eq. (2.12) into two parts, quark-quark and quark-antiquark terms, and adopt an averaged value for the parameter μ in each, μ_{qq} and $\mu_{q\bar{q}}$. Using the wave function in Eqs. (2.2)-(2.5) we find that the relevant spin-flavor-color matrix elements are given by

$$\begin{aligned}
\langle 1,\overline{10},1/2|\sum_{i<j\neq 5}\lambda_i\cdot\lambda_j\,\sigma_i\cdot\sigma_j\,|1,\overline{10},1/2\rangle &= 16/3 \\
\langle 1,\overline{10},1/2|\sum_{i<j=5}\lambda_i\cdot\lambda_j\,\sigma_i\cdot\sigma_j\,|1,\overline{10},1/2\rangle &= 40/3\ ,
\end{aligned} \tag{2.13}$$

where $j = 5$ corresponds to the antiquark. This evaluation was done by group theoretic techniques [53], as well as brute-force symbolic manipulation [59]. To understand how we evaluate the coefficients μ_{qq} and $\mu_{q\bar{q}}$ let us consider a nucleon-like state in the antidecuplet, the p_5. The probability of finding an $s\bar{s}$ pair in the p_5 state is $2/3$. In this case, $1/2$ of the possible qq pairs will involve a strange quark. On the other hand, the probability that the p_5 will contain five non-strange constituents is $1/3$. Thus, we take

$$\mu_{qq}(p_5) = \frac{2}{3}[\frac{1}{2}(\mu(0,0)+\mu(0,m_s))] + \frac{1}{3}\mu(0,0)\ . \tag{2.14}$$

By similar reasoning,

$$\mu_{q\bar{q}}(p_5) = \frac{1}{3}\mu(0,0) + \frac{1}{2}\mu(0,m_s) + \frac{1}{6}\mu(m_s,m_s) \ . \tag{2.15}$$

We also use the averaged kinetic energy terms

$$\frac{2}{3R}[3\Omega(0) + 2\Omega(m_s)] + \frac{1}{3R}[5\Omega(0)] \ . \tag{2.16}$$

The bag mass prediction is then obtained by numerically minimizing the mass formula with respect to the bag radius R. Applying this procedure to the p_5 and Θ^+ states, we find the antidecuplet mass splitting

$$\Delta M_{\overline{10}} \approx 52 \text{ MeV}. \tag{2.17}$$

We use the observed Θ^+ mass, 1542 MeV, and the splitting $\Delta M_{\overline{10}}$ to estimate the masses of the p_5, Σ_5, and Ξ_5 states; we find 1594, 1646, and 1698 MeV, respectively. Decay predictions from SU(3) symmetry are summarized in Table 2.1.

While we used the bag model as a framework for evaluating the mass spectra above, we believe our results are typical of any constituent quark model.

We adopt a simpler approach in evaluating the effect of spin-isospin constituent interactions,

$$\Delta M_{SI} = -C_\chi \langle 1, \overline{10}, 1/2| \sum_{i<j} \tau_i \cdot \tau_j \ \sigma_i \cdot \sigma_j \, |1, \overline{10}, 1/2\rangle \ . \tag{2.18}$$

In this case the flavor generators τ are Pauli matrices, and the coefficient $C_\chi = 25 - 30$ MeV is determined from the $N - \Delta$ mass splitting; we use 30 MeV [58]. The dimensionless matrix element can be computed using Eqs. (2.2)-(2.5), and we find 10, 20/3, 25/9 and $-5/3$ for the Θ^+, p_5, Σ_5 and the Ξ_5, respectively. The mass splitting due to the strange quark constituent mass can be estimated from our previous bag model calculation, by excluding the spin-color interactions, yielding $\Delta M_s \approx 55$ MeV. Again fixing the Θ^+ mass at 1542 MeV, we then find 1697, 1869, and 2058 MeV for the p_5, Σ_5, and Ξ_5 mass, respectively. Decay results for this mass spectrum are also presented in Table 2.1. Note

that a number of the decay modes that were kinematically forbidden before are allowed if spin-isospin interactions dominate, due to the larger predicted splitting within the antidecuplet. (For a smaller choice of $C_\chi \approx 25$ MeV, the ΣK modes are still inaccessible.)

Decay	$\lvert A/A_0\rvert^2$	Γ/Γ_0 (SC)	Γ/Γ_0 (SI)
$\Theta^+ \to pK^0$	1	0.99	0.99
$p_5 \to \Lambda K^+$	1/2	–	0.49
$p_5 \to p\eta$	1/2	0.50	0.68
$p_5 \to \Sigma^+ K^0$	1/3	–	0.12
$p_5 \to \Sigma^0 K^+$	1/6	–	0.06
$p_5 \to n\pi^+$	1/3	0.63	0.68
$p_5 \to p\pi^0$	1/6	0.32	0.34
$\Sigma_5^+ \to \Xi^0 K^+$	1/3	–	0.30
$\Sigma_5^+ \to \Sigma^+ \eta$	1/2	–	0.62
$\Sigma_5^+ \to \Lambda\pi^+$	1/2	0.89	1.11
$\Sigma_5^+ \to p\bar{K}^0$	1/3	0.45	0.63
$\Sigma_5^+ \to \Sigma^+\pi^0$	1/6	0.27	0.36
$\Sigma_5^+ \to \Sigma^0\pi^+$	1/6	0.27	0.36
$\Xi_5^+ \to \Xi^0\pi^+$	1	1.47	2.37
$\Xi_5^+ \to \Sigma^+\bar{K}^0$	1	0.36	1.99

TABLE 2.1: SU(3) decay predictions for the highest isospin members of the antidecuplet. A_0 and Γ_0 are the amplitude and partial decay width for $\Theta^+ \to NK^+$, respectively; SC and SI indicate antidecuplet mass spectra assuming dominant spin-color or spin-isospin constituent interactions.

The Skyrme model also has predictions [51] for the masses and decays of the antidecuplet. The mass splittings there were about 180 MeV between each level of the decuplet (with the Θ^+ still the lightest), considerably larger splittings than we find in a constituent quark model where the mass splittings come from strange quark masses and from color-spin interactions. Mass splittings using isospin-spin interactions were, on the other hand, more comparable to the Skyrme model results.

Decays of the antidecuplet into a ground state octet baryon and an octet meson involve a decay matrix element and phase space. Ratios of decay matrix elements for pure antidecuplets, such as we show in Table I, are fixed by $SU(3)_F$ symmetry. They are the same in any model, as may be confirmed by comparing Table I to results in [51]. We have

neglected mixing; Ref. [51] does consider mixing but does not find large consequences for the decays. The differences between relative decay predictions are then due to differences in phase space, and the differences are due to masses and due to parity. Negative parity states decaying to ground state baryon and pseudoscalar meson have S-wave phase space, while positive parity states have P-wave phase space. Note also that $SU(3)_F$ symmetry does not allow decays of antidecuplets into decuplet baryons plus octet mesons.

2.4 Discussion

In this chapter we have shown how to construct the quark model wave functions for members of the pentaquark antidecuplet, the flavor multiplet that we argue is most likely to contain the strangeness one state recently observed in a number of experiments [1, 2, 5]. We present two decompositions of the $\overline{10}$ wave function that are useful for computing spin-flavor-color matrix elements, and that reveal the hidden strangeness in each component state. In addition, we have presented the Θ^+ wave function in explicit form. We use these results to estimate the effect of spin-color and spin-isospin interactions on the pentaquark mass spectrum. In the first case, we use the MIT bag as a representative constituent quark model to compute the equal spacing between antidecuplet states that differ by one unit of strangeness; we estimate a splitting of 52 MeV. The observed Θ^+ mass and SU(3) symmetry then allows us to make decay predictions. Notably, if only color-spin interactions are present, decays of the p_5 and Σ_5 to final states in which both decay products have nonzero strangeness are kinematically forbidden. In addition, the Ξ_5 states are narrower than those in Ref. [51], so that experimental detection might be possible and dramatic. If instead, spin-isospin interactions dominate, all the decays in Table 2.1 become kinematically accessible.

The work summarized here sets the groundwork for further investigation. Of particular interest to us is the relation between bag model predictions for the absolute pen-

taquark mass (rather than the mass splittings considered here) and the mass of other multiquark exotic states. The conventional MIT bag predicts a Θ^+ mass that is too large relative to the experimental value (we find that a prediction of about 1700 MeV is typical); however, these numbers can be easily reconciled by allowing bag model parameters to float [56, 57]. An appropriate analysis requires a simultaneous fit to pentaquark and low-lying non-exotic hadron masses, and consideration of center-of-mass corrections. Whether such fits simultaneously allow for sufficiently heavy six-quark states, given a choice of constituent interactions, is an open question. Our analysis also gives insight into other pentaquark states. For example, there are nucleon-like states in the pentaquark octet (states in the same spin-color representation as the Θ^+) which are potentially light. However, we find that these states also have hidden strangeness, placing them within one-third of the strange quark mass below the Θ^+, if no other effects are considered, and at or above the Θ^+ mass if spin-isospin interactions are taken into account. This is one example of the value of extending our present analysis to other pentaquark multiplets. A more detailed discussion of these topics, as well as of the group theoretical issues described here will be presented in chapter 3.

CHAPTER 3

Positive Parity Pentaquarks Pragmatically Predicted

3.1 Introduction

There are a number of pre-discovery theoretical studies of pentaquarks [32, 33, 34, 35, 49, 50, 51, 60], some including heavy quarks in the pentaquark state [36, 37, 38]. Of particular note is [51], which, though it has been criticized [61, 62], advanced the field by predicting in the context of a chiral soliton model a narrow pentaquark only 10 MeV away from the discovery mass. Since the Θ^+ discovery, there has been a flurry of papers studying pentaquark properties in constituent quark models [31, 40, 41, 45, 63, 64, 65, 66], other aspects of pentaquarks in soliton models [42, 44, 48, 62, 67], production of pentaquarks, including in heavy ion collisions [16, 17, 68, 69, 70, 71], non-observance of pentaquarks in earlier hadronic experiments [47, 72, 73], pentaquarks in the large N_c limit [74], and other pentaquark topics [39, 75, 76, 77, 78].

At present, the spin and parity of the Θ^+ are experimentally unknown. A majority of the theoretical papers, including all the chiral soliton papers, treat the state as positive

parity. A minority, including an earlier work by the present authors [65], have considered the possibility of negative parity [78]. All theory papers, to our knowledge, consider the Θ^+ to be spin-1/2. Regarding the isospin, a Θ^{++} signal has been sought and not found [3], so that the Θ^+ appears to be isoscalar and hence a member of a pentaquark flavor antidecuplet.

In this chapter, we focus on understanding how a positive parity state could emerge as the lightest pentaquark, in the context of a constituent quark model [31, 66, 79]. We explore the consequences of the ensuing picture for other states in the pentaquark antidecuplet. Positive parity pentaquarks in a constituent quark model require a negative-parity spatial wave function, obtained by putting one quark in the lowest P-state of a suitable collective potential. One could entertain more complicated excited state scenarios also (e.g., [43]). Here we discuss a plausible mechanism that changes the level ordering so that a state with an excited wave function becomes the lightest one. In this approach, the positive parity of the state is a consequence of the quark-quark pairwise potential and the chosen symmetry structure of the flavor-spin wave function.

Insight comes from studies of three-quark baryons [58], where the level ordering of the first excited positive and negative parity states is reproduced correctly in an effective theory where the dominant pairwise interaction is flavor-spin dependent. One-gluon exchange gives only a color-spin dependent force. Flavor-spin dependent interactions can be pictured as arising from the interchange of quark-antiquark pairs with the quantum numbers of pseudoscalar mesons. However, the effective theory viewpoint does not require that one commit to a specific model for the underlying physics. Skyrmion or instanton induced interactions could be described equally well by the effective field theory introduced below.

In the next section, we demonstrate how effective flavor-spin interactions lead to the correct q^3 mass spectrum, and in particular rectify the level order of the Roper and negative parity resonances. We also discuss semiquantitatively the consequences of the

flavor-spin interaction for the pentaquark system. Section 3.3 includes a more detailed numerical analysis, taking into account the breaking of $SU(3)_F$ symmetry. We give predictions which are new in the effective theory context for the mass and decays widths of other members of the pentaquark antidecuplet, particularly the exotic cascade states Ξ_5. In a constituent quark model with flavor independent spin-splittings, the difference between the Ξ_5 and Θ^+ masses is just that obtaining from an additional strange quark, about 150 MeV [43, 65]. We find that the flavor symmetry breaking stretches out this mass gap considerably, pushing the Ξ_5 mass to about 1900 MeV. This is nonetheless much smaller than the mass gap predicted in the chiral soliton model in [51]. The predicted width of a 1900 MeV Ξ_5 is still narrow, which suggests that the Ξ_5 should be distinguishable from background.

3.2 Framework

A key feature of the flavor-spin interaction is that it is most attractive for states that have the most symmetric flavor-spin wave functions. If the interaction has exact $SU(3)_F$ flavor symmetry (which may not be the case and which we do not assume later), then the mass shift is given by

$$\Delta M_\chi = -C_\chi \sum_{\alpha<\beta} (\lambda_F \sigma)_\alpha \cdot (\lambda_F \sigma)_\beta \ , \tag{3.1}$$

where the sum is over all qq and $q\bar{q}$ pairs (α, β), the $\vec{\sigma}_\alpha$ are Pauli spin matrices for quark or antiquark α, and $\vec{\lambda}_{F\alpha}$ are flavor Gell-Mann matrices. Coefficient C_χ is a positive number. Let us focus on states or components of states that contain quarks only. If the flavor-spin state is symmetric overall, then one may write the wave function as a sum of terms in which a given pair of quarks is singled out and in which the individual spin and flavor wave functions of the given pair are either both symmetric or both antisymmetric. In either case, the expectation values of $\vec{\sigma}_\alpha \cdot \vec{\sigma}_\beta$ and $\vec{\lambda}_{F\alpha} \cdot \vec{\lambda}_{F\beta}$ for that pair have the same

sign and yield maximal attraction.

The most significant contribution to Eq. (3.1) in a pentaquark state comes from the sum over the q^4 component. Let us compare the situation of four quarks in S-states $[S^4]$ to one where one quark is in a P-state and three are in S-states $[S^3P]$. The color state of the q^4 must be a 3, which for four quarks is a mixed symmetry state. If all quarks are in the same spatial state, then of necessity the flavor-spin state must also be of mixed symmetry. However, for the S^3P combination, one can have a mixed-symmetry spatial state and a color-orbital state that is totally antisymmetric. The flavor-spin wave function is then totally symmetric, and leads to the most attractive possible flavor-spin interaction. We will compute below the numerical lowering of the S^3P binding energy relative to the S^4, and show that it is dramatically large, more than enough to balance the extra energy associated with the orbital excitation. This gives a semiquantitative understanding of the numerical results that we present in section 3.3.

It is useful to recall how flavor-spin interactions work in the ordinary q^3 baryon systems, both to motivate our framework and to estimate numerical values for the parameters involved. The dramatic problem that is solved is the level ordering of the $N^*(1440)$, the positive parity S-state excitation of the nucleon also known as the Roper resonance, and the $N^*(1535)$, the lightest spin-1/2 negative parity resonance, which we refer to as the S_{11}.

In the Bag model and in linear or harmonic oscillator confining potentials, the first excited S-state lies above the lowest P-state, making the predicted Roper mass heavier than the lightest negative parity baryon mass. Pairwise spin-dependent interactions must reverse the level ordering. As mentioned earlier, color-spin interactions fail in this regard [80], while flavor-spin interactions produce the desired effect. Since the q^3 color wave function is antisymmetric, the flavor-spin-orbital wave function is totally symmetric. For all quarks in an S-state, the flavor-spin wave function is totally symmetric all by itself and leads to the most attractive flavor-spin interaction. If one quark is in a P-state,

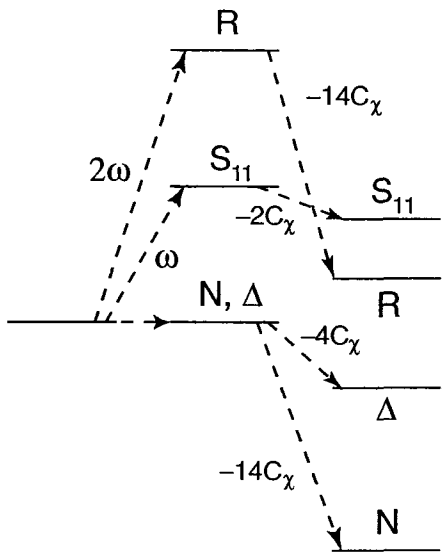

FIG. 3.1: Schematic view of the level reversal of the P-state and excited S-state for 3-quark baryons.

the orbital wave function is mixed symmetry and so is the flavor-spin wave function, and the flavor-spin interaction is a less attractive . In the $SU(3)_F$ symmetric case, Eq. (3.1), one obtains mass splittings

$$\Delta M_\chi = \begin{cases} -14C_\chi & N(939), N^*(1440) \\ -4C_\chi & \Delta(1232) \\ -2C_\chi & N^*(1535) \end{cases} . \tag{3.2}$$

Here we have approximated the $N^*(1535)$ as a state with total quark spin-1/2.

The scenario is shown in Fig. 3.1. Relative to some base mass, one first has the 2S–1S and 1P–1S splittings for the Roper and the S_{11}. Then the flavor-spin pairwise interactions further split the spectrum into its final form, placing the Roper below the mass of the negative parity baryon. We have worked with a small number of states to illustrate clearly how the mechanism works. More extensive evidence that flavor-spin splitting is significant in the baryon spectrum is found in [58, 81, 82, 83, 84, 85, 86, 87, 88, 89].

Returning to pentaquarks, the presence of a P-state now allows for a more rather than a less symmetric q^4 flavor-spin wave function. The net result is that pentaquarks

with S^3P four-quark components are lighter than the corresponding states with all quarks in the ground state. One can estimate the advantage of this configuration as follows. For the q^4 part of the state, the mass splitting of Eq. (3.1) evaluates to,

$$\Delta M_\chi = -C_\chi \left\{ 4C_6(R) - 8N - \frac{4}{3}S^2 - 2F^2 \right\} , \tag{3.3}$$

where $C_6(R)$ is the quadratic Casimir of the $SU(6)$ flavor-spin representation R, N is the number of quarks, and S^2 and F^2 are the spin and flavor quadratic Casimirs of the state. (We normalize generators Λ_A so that Tr $\Lambda_A\Lambda_B = (1/2)\delta_{AB}$. A representation R can be specified by its Young diagram, and a useful expression for the quadratic Casimir of representations of $SU(Q)$ is found in [90],

$$C_Q(R) = \frac{1}{2}\left(NQ - \frac{N^2}{Q} + \sum r_i^2 - \sum c_i^2 \right) \tag{3.4}$$

where r_i is the number of boxes in the i^{th} row of the Young diagram, c_i is the number of boxes in the i^{th} column, and N is the total number of boxes.) For the present situation,

$$\Delta M_\chi = \begin{cases} -\frac{28}{3}C_\chi & S^4 \\ -28C_\chi & S^3P \end{cases} . \tag{3.5}$$

To make a Θ^+, all four quarks are non-strange and the state is isospin-0. Fermi symmetry requires the S^4 state to be spin-1. The S^3P state can be spin-0, and we take it so. Thus

$$M(S^3P) - M(S^4) = \hbar\omega - \frac{56}{3}C_\chi \approx -310 \text{ MeV} . \tag{3.6}$$

For the numerical evaluation of Eq. (3.6), we have assumed the $1P$–$1S$ level splitting of a harmonic oscillator potential, with $2\hbar\omega$ estimated from the nucleon-Roper mass difference; the coefficient C_χ is fixed by the nucleon-$\Delta(1232)$ mass splitting. Adding the strange antiquark to the spin-0 S^3P state gives no further spin-dependent mass shift. Adding the $\bar{s}$ to the spin-1 S^4 state does give a spin-dependent splitting and can lower the mass, but not decisively. Thus, the pentaquark state with an S^3P four-quark state is the lightest by a wide margin.

A key concern is the location of the other pentaquark states. Particularly interesting are the other exotic members of the pentaquark antidecuplet, namely the isospin-3/2 pentaquark Ξ_5, or cascade, states. To more accurately predict the masses and widths of these strangeness -2 states, or of other states of varying flavor, we should consider the effects of flavor symmetry breaking in the flavor-spin interaction. Certainly one knows that isolated quark-antiquark pairs bind into states with flavor-dependent masses. With flavor symmetry breaking we write the isospin-conserving, spin-dependent interaction as

$$\Delta M = -C_{SI}\sum_{\alpha<\beta}(\tau\sigma)_\alpha\cdot(\tau\sigma)_\beta - C_{47}\sum_{\alpha<\beta,i=4}^{7}(\lambda^i\sigma)_\alpha\cdot(\lambda^i\sigma)_\beta - C_8\sum_{\alpha<\beta}(\lambda^8\sigma)_\alpha\cdot(\lambda^8\sigma)_\beta\,. \tag{3.7}$$

The τ_α^i are the isospin matrices for quark α, the same as λ_α^i for $i = 1,2,3$. We find the coefficients by studying the mass splitting in the three-quark sector, as is reported in the next section. Matrix elements of Eq. (3.7) in the pentaquark states (summing over all 5 constituents) are also presented, so that the splittings within the pentaquark antidecuplet are easily obtained.

3.3 Fits and Predictions

In the previous section, the significance of the flavor-spin interactions in establishing the correct level ordering for the Roper and N*(1535) resonances was pointed out. Here we will focus on the effects of flavor-spin interactions in the case where $\mathrm{SU}(3)_F$ is broken both by the strange quark mass and by the flavor-spin interactions when C_{SI}, C_{47}, and C_8 in Eq. (3.7) are unequal. We consider three quark systems first to determine the relevant parameters.

We obtain the values for coefficients in Eq. (3.7) by fitting the mass spectrum of the low-lying octet and decuplet baryons. For a specific q^3 state the mass M is given by

$$M = M_0^{(3)} + x_1 C_{SI} + x_2 C_{47} + x_3 C_8 + n_s \Delta m_s\,, \tag{3.8}$$

where $M_0^{(3)}$ is a base mass, x_1, x_2, and x_3 are matrix elements of the operators in Eq. (3.7), n_s is the number of strange quarks, and Δm_s is the mass increase due to the presence of a strange quark.

State	x_1	x_2	x_3	n_s
N	-15	0	1	0
Δ	-3	0	-1	0
Λ	-9	-6	1	1
Σ	-1	-10	-3	1
Σ^*	-1	-4	1	1
Ξ	0	-10	-4	2
Ξ^*	0	-4	0	2
Ω	0	0	-4	3

TABLE 3.1: Numerical coefficients for Eq. (3.8).

We fit $M_0^{(3)}$, Δm_s, C_{SI}, C_{47} and C_8 to the well-known masses of the baryons listed in Table 3.2. The experimental masses given are isospin averages. The results are:

$$\begin{aligned} M_0^{(3)} &= 1340.5 \pm 5.3 \text{ MeV}, \quad \Delta m_s = 136.3 \pm 2.5 \text{ MeV} \\ C_{SI} &= 28.2 \pm 0.5 \text{ MeV}, \quad C_{47} = 20.7 \pm 0.5 \text{ MeV}, \quad C_8 = 19.7 \pm 1.2 \text{ MeV} . \end{aligned} \tag{3.9}$$

An error of 5 MeV is assumed for each of the baryon masses, to take into account theoretical uncertainties. Thus, moving any of the parameters to the edge of the quoted error limits changes the predicted baryon masses by about 5 MeV. With these parameters, and the Roper fixed at 1440 MeV, the S_{11} mass is predicted to be 1526 MeV.

Applying the same approach to the pentaquark antidecuplet, we obtain a mass M for each state given by:

$$M = M_0^{(5)} + x_1 C_{SI} + x_2 C_{47} + x_3 C_8 + n_s^{eff} \Delta m_s \, . \tag{3.10}$$

$M_0^{(5)}$ is the base mass for 5-quark bound states and should be different from $M_0^{(3)}$ found earlier. The values for model parameters given in Eq. (3.8) can change in going from q^3

State	Experimental Mass (MeV)	Predicted Mass (MeV)
N	939	937
Δ	1232	1236
Λ	1116	1119
Σ	1193	1183
Σ^*	1385	1386
Ξ	1318	1327
Ξ^*	1533	1530
Ω	1672	1670

TABLE 3.2: Fit to the low-lying octet and decuplet baryon masses, using the predictions given by Eq. (3.7) and Table 3.1.

system to $q^4\bar{q}$ system. We anticipate that the largest change in the model parameters will occur in M_0, while we expect the other parameters to have a less marked dependence on the number of quarks. Therefore we proceed by eliminating $M_0^{(5)}$ from the mass formula by the use of the experimentally measured mass of the Θ^+, M_Θ=1542 MeV [1, 2, 3, 4, 5]. The number n_s^{eff}, is the expectation value of the number of strange quarks plus strange antiquarks in each state, taking due account of hidden strangeness components, which were shown to be significant in [65]. The necessary matrix elements may be evaluated using the pentaquark maximally symmetric flavor-spin wave function, which can be written as[1]

$$\left|(\overline{10},1/2)\right\rangle = \frac{1}{\sqrt{2}}\left|(\bar{3},0)(\bar{3},0)\right\rangle_{\bar{6},0} + \frac{1}{\sqrt{2}}\left|(6,1)(6,1)\right\rangle_{\bar{6},0}\ , \tag{3.11}$$

where the pair of numbers in parentheses refer to the flavor and spin. On the right hand side, the first (second) pair of numbers refers to the first (second) pair of quarks, and the quantum numbers of the antiquark $(\bar{3},1/2)$ are the same in each term and have been suppressed. The numerical values of the matrix elements in Eq. (3.10) are given in Table 3.3.

[1]The four-quark part of this state is totally antisymmetric, as it should be. A diquark-diquark state, such as in [43], has antisymmetry within each diquark, but antisymmetry when exchanging quarks between different diquarks is not enforced. This can be viewed as an approximation that is valid if the diquarks are much smaller than the overall state. In a absence of a mechanism that compresses the diquarks, a diquark-diquark state violates Fermi-Dirac statistics.

State	x_1	x_2	x_3	n_s^{eff}
Θ	-30	0	2	1
N_5	-20	-8	0	$\frac{4}{3}$
Σ_5	$-\frac{31}{3}$	$-\frac{44}{3}$	-3	$\frac{5}{3}$
Ξ_5	-1	-20	-7	2

TABLE 3.3: Numerical coefficients for Eq. (3.10).

Using the wave function given by Eq. (3.11), and the mass formula expressed in Eq. (3.10), we find the following masses for the members of the baryon antidecuplet: $M(N_5) = 1665$ MeV, $M(\Sigma_5) = 1786$ MeV and $M(\Xi_5) = 1906$ MeV. To complete our predictions, we use the predicted mass spectrum and $SU(3)_F$ symmetry for the decay matrix elements to estimate widths of the decay modes of the highest isospin members of the antidecuplet. Table 3.4 lists our predictions.

Decay	$\lvert A/A_0\rvert^2$	Γ/Γ_0	Decay	$\lvert A/A_0\rvert^2$	Γ/Γ_0
$\Theta^+ \to pK^0$	1	0.97	$\Sigma_5^+ \to \Sigma^+\eta$	1/2	0.13
$p_5 \to \Lambda K^+$	1/2	0.15	$\Sigma_5^+ \to \Lambda\pi^+$	1/2	2.63
$p_5 \to p\eta$	1/2	1.10	$\Sigma_5^+ \to p\bar{K}^0$	1/3	1.86
$p_5 \to \Sigma^+K^0$	1/3	–	$\Sigma_5^+ \to \Sigma^+\pi^0$	1/6	0.63
$p_5 \to \Sigma^0K^+$	1/6	–	$\Sigma_5^+ \to \Sigma^0\pi^+$	1/6	0.61
$p_5 \to n\pi^+$	1/3	2.48	$\Xi_5^+ \to \Xi^0\pi^+$	1	3.23
$p_5 \to p\pi^0$	1/6	1.25	$\Xi_5^+ \to \Sigma^+\bar{K}^0$	1	2.22
$\Sigma_5^+ \to \Xi^0K^+$	1/3	–			

TABLE 3.4: SU(3) decay predictions for the highest isospin members of the positive parity antidecuplet. A_0 and Γ_0 are the amplitude and partial decay width for $\Theta^+ \to nK^+$, respectively. Pentaquark masses are 1542, 1665, 1786, and 1906 MeV, for the Θ^+, p_5, Σ_5 and Ξ_5, respectively.

It should be stressed that we view the mass and decay predictions of the Ξ_5 states to be most reliable due to the absence of substantial mass mixing with nearby states. While we provide predictions for the N_5 and Σ_5 for the sake of completeness, these may be subject to large corrections due to mixing with octet pentaquarks. Whether such effects could be reliably evaluated is an interesting question which is beyond the scope of the present work.

3.4 Conclusions

We have considered the possibility that the lightest strangeness one pentaquark state is positive parity, with one unit of orbital angular momentum. In this case, it is possible to construct states with totally symmetric spin-flavor wave functions. Spin-flavor exchange interactions, if dominant, render these states lighter than any pentaquark with all its constituents in the ground states. We assume such spin-flavor exchange interactions in an effective theory, including flavor SU(3) breaking effects in operator coefficients and in the quark masses. The general form of these multi-quark interactions is consistent with a number of possible models of the underlying dynamics, including pseudoscalar meson exchange, skyrmions, and instanton-induced effects. In our approach, however, we need not commit ourselves to any specific dynamical picture. We believe that the theoretical uncertainty in using such a streamlined (yet pragmatic) approach is no greater than the spread in predictions between different specific models. Use of effective spin-flavor exchange interactions is well motivated given its success in explaining the lightness of the Roper resonance relative to the negative parity N(1535), as we demonstrated in Section 3.2. Simple quark models without dominant spin-flavor exchange interactions simply get the ordering of these states wrong. Fitting our operator coefficients, a mean multiplet mass, and a strangeness mass contribution to the masses of the ground state octet and decuplet baryons, we then predict mass splittings in the parity even pentaquark antidecuplet. In particular, our approach allows us to predict the mass of the strangeness -2 cascade states at 1906 MeV, with a full width approximately 2.8 times larger than that of the Θ^+. The cascade states do not mix with any other pentaquarks of comparable mass, which makes these prediction particularly robust. Discovery of cascade pentaquarks around 1906 MeV would therefore provide an independent test of the importance of spin-flavor exchange interactions in the breaking of the approximate SU(6) symmetry of the low-lying hadron spectrum.

CHAPTER 4

A Naturally Narrow Positive Parity Θ^+

4.1 Introduction

Pentaquarks are baryons whose minimal Fock components consist of four quarks and an antiquark. The first observed pentaquark was the $\Theta^+(1540)$ with strangeness $S = +1$, and with quark content $uudd\bar{s}$. More recently, the NA49 Collaboration [91] has reported a narrow $\Xi_5^{--}(1860)$ baryon with $S = -2$ and quark content $dsds\bar{u}$, together with evidence for its isoquartet partner Ξ_5^0 at the same mass. All but one theoretical paper [39] treat the Θ^+ as an isosinglet. If the Θ^+ were a member of an isovector or isotensor multiplet, then one would expect to observe its doubly charged partner experimentally. The SAPHIR Collaboration [3] searched for a Θ^{++} in $\gamma p \to \Theta^{++}K^- \to pK^+K^-$, with negative results. They concluded that the Θ^+ is an isosinglet and hence a member of a pentaquark antidecuplet.

The spin and parity quantum numbers of the Θ^+ have yet to be determined experimentally. The spin of Θ^+ is taken to be 1/2 by all theory papers to our knowledge and various estimates show that spin-3/2 pentaquarks must be heavier [44, 48, 67, 92, 93]. A more controversial point among theorists is the parity of the state. For example, QCD

sum rule calculations [45], quenched lattice QCD [77], and a minimal constituent quark treatment by the present authors [65], predict that the lightest Θ^+ is a negative parity isosinglet. All chiral soliton papers [51, 61], some correlated quark models [41, 43], and some works within the constituent quark model [31, 66, 79, 94] including a second work by the present authors [53], predict the lightest Θ^+ pentaquark as a positive parity isosinglet.

The photoproduction and the pion-induced production cross sections of the Θ^+ were studied in [71, 95, 96, 97]. It was shown in both cases that the production cross sections for a negative parity Θ^+ are much smaller than those for the positive parity state (for a given Θ^+ width). In Ref. [71, 95, 96, 97], results for the Θ^+ production cross section in photon-proton reactions were compared with estimates of the cross section based on data obtained by the SAPHIR Collaboration [3], and odd-parity pentaquark states were argued to be disfavored.

In this chapter, we present new results following from a consistent treatment of the color-flavor-spin-orbital wave function for a positive parity Θ^+. In [53] (inspired by [31, 94]), we showed that dominant flavor-spin interactions render the positive parity Θ^+ lighter than its negative parity counterpart. Here we will present decompositions of the quark model wave function of the Θ^+, explicitly including the orbital part. We will see that the narrowness of the Θ^+ follows naturally from the group theoretic structure of the state.

4.2 Wave Function

If flavor-spin interactions dominate [58], the lightest positive parity Θ^+ will have a flavor-spin (FS) wave function that is totally symmetric [31, 53, 66, 94]. Fermi-Dirac statistics dictates that the color-orbital (CO) wave function must be fully antisymmetric. We present two decompositions of the wave function, one in terms of quark pairs and the

antiquark, and another in terms of the quantum numbers of q^3 and $q\bar{q}$ subsystems.

In the first decomposition, the overall q^4 flavor state must be a $\bar{\mathbf{6}}$. This is the only representation that one can combine with a flavor $\bar{\mathbf{3}}$ (the antiquark) to form an antidecuplet. This further implies that the overall q^4 spin is 0, since the only possible fully symmetric q^4 (F,S) wave functions are $(\bar{\mathbf{6}},0)$ or $(\mathbf{15}_{\mathrm{M}},1)$. A flavor $\bar{\mathbf{6}}$ can be obtained if both quarks pairs are in either a $\mathbf{6}$ or $\bar{\mathbf{3}}$, while a spin-0 state can be obtained if both are either spin-0 or 1. Since we want a fully symmetric FS wave function, we must combine these possibilities as follows:

$$|FS\rangle_{(\bar{\mathbf{6}},0)} = a\,|(\bar{\mathbf{3}},0)(\bar{\mathbf{3}},0)\rangle_{(\bar{\mathbf{6}},0)} + b\,|(\mathbf{6},1)(\mathbf{6},1)\rangle_{(\bar{\mathbf{6}},0)}\ . \tag{4.1}$$

The parentheses on the right hand side delimit the flavor and spin quantum numbers of the first and second pair of quarks, each of which is combined into an overall $(\bar{\mathbf{6}},0)$. For the Θ^+, the q^4 states on the right-hand-side are:

$$\begin{aligned}
|(\bar{\mathbf{3}},0)(\bar{\mathbf{3}},0)\rangle_{(\bar{\mathbf{6}},0)} &= \frac{1}{4}(ud-du)(ud-du)\otimes(\uparrow\downarrow-\downarrow\uparrow)(\uparrow\downarrow-\downarrow\uparrow)\,,\\
|(\mathbf{6},1)(\mathbf{6},1)\rangle_{(\bar{\mathbf{6}},0)} &= \frac{1}{12}(2uudd+2dduu-udud-uddu-duud-dudu)\\
&\otimes\ \left(2\uparrow\uparrow\downarrow\downarrow+2\downarrow\downarrow\uparrow\uparrow-\uparrow\downarrow\uparrow\downarrow-\uparrow\downarrow\downarrow\uparrow-\downarrow\uparrow\uparrow\downarrow-\downarrow\uparrow\downarrow\uparrow\right).
\end{aligned} \tag{4.2}$$

Total symmetry of the wave function demands $a = b$. To properly normalize the state, we choose $a = b = 1/\sqrt{2}$.

The next step is to construct the totally antisymmetric CO wave function. The q^4 color state must be a $\mathbf{3}$, which is a mixed symmetry state, whose Young tableaux is shown in Fig. 4.2. The orbital state, containing three S-states and one P-state, must have a permutation symmetry given by the conjugate tableaux in order to obtain overall antisymmetry. Hence the structure of our wave functions implies that the strange antiquark is not orbitally excited; simple estimates suggest that a state with the $\bar{s}$ excited would be considerably heavier [53]. The possible color and orbital representations for two pairs of quarks are shown in Fig. 4.2.

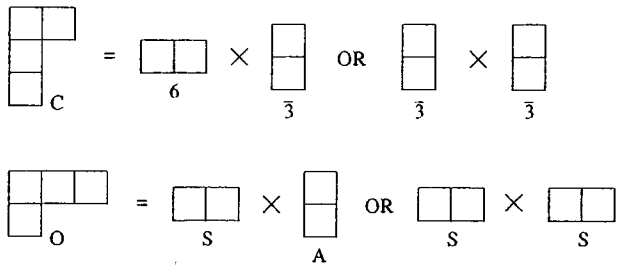

FIG. 4.1: All possible states that can be appropriately combined to yield a totally antisymmetric CO state

From Fig. 4.2, a totally antisymmetric CO wave function must have the form:

$$|CO\rangle = a'\,|(\bar{\mathbf{3}},\mathbf{S})(\bar{\mathbf{3}},\mathbf{S})\rangle + b'\{|(\mathbf{6},\mathbf{A})(\bar{\mathbf{3}},\mathbf{S})\rangle + |(\bar{\mathbf{3}},\mathbf{S})(\mathbf{6},\mathbf{A})\rangle\}\,. \tag{4.3}$$

The coefficients a' and b' are fixed by the constraint that the wave function must be antisymmetric under interchange of the first and third quarks. When the q^4 color state is red, the explicit expressions for the wave functions on the right-hand-side are:

$$\begin{aligned}
|(\bar{\mathbf{3}},\mathbf{S})(\bar{\mathbf{3}},\mathbf{S})\rangle &= \frac{1}{\sqrt{8}}\{(RG-GR)(BR-RB)-(BR-RB)(RG-GR)\} \\
&\otimes \frac{1}{2}\{SS(SP+PS)-(SP+PS)SS\}\,, \\
|(\mathbf{6},\mathbf{A})(\bar{\mathbf{3}},\mathbf{S})\rangle &= \frac{1}{4}\{(2RR(GB-BG)+(RG+GR)(BR-RB) \\
&\qquad +(RB+BR)(RG-GR)\} \\
&\otimes \frac{1}{\sqrt{2}}(SP-PS)SS\,.
\end{aligned} \tag{4.4}$$

The wave function is properly normalized with the choice $a' = b' = 1/\sqrt{3}$. In our construction, the total spin of the $q^4\bar{q}$ can only be $1/2$. Appropriate Clebsch-Gordan coefficients may be chosen to combine the orbital angular momentum of the excited q so that the total Θ^+ spin is $1/2$. We leave this implicit.

For the second decomposition, we note that the q^3 and $q\bar{q}$ flavor wave functions must both be 8's if one is to form a flavor $\overline{10}$. Since the q^4 FS wave function is fully symmetric, the q^3 FS wave function must be fully symmetric also. The mixed symmetry

of the q^3 flavor wave function implies that the q^3 spin wave function must have mixed symmetry also and hence is spin-1/2. Total symmetrization of the q^3 FS wave function is obtained as follows:

$$|(8,1/2)\rangle_{q^3} = \frac{1}{\sqrt{2}}\Big[\,|(8_S,1/2_S)\rangle + |(8_A,1/2_A)\rangle\,\Big]\,, \tag{4.5}$$

where the subscripts S and A refer to the permutation symmetry of the first two quarks. The $q\bar{q}$ spin can be 0 or 1. The fully symmetric FS wave function is of the form

$$|FS\rangle_{(\overline{10},1/2)} \;=\; a''\,|(8,1/2)(8,0)\rangle_{(\overline{10},1/2)} + b''\,|(8,1/2)(8,1)\rangle_{(\overline{10},1/2)}\,, \tag{4.6}$$

where the coefficients a'' and b'' are fixed by requiring that the wave function is symmetric under the interchange of the first and fourth quarks. For the Θ^+, the part of the states on the right-hand-side that have z-component spin projection $1/2$ are:

$$\begin{aligned}
|(8,1/2)(8,0)\rangle_{(\overline{10},1/2)} \;=\; & \frac{1}{\sqrt{2}}\Big[\frac{1}{4}(ud-du)(ud-du)\bar{s}\otimes(\uparrow\downarrow-\downarrow\uparrow)\uparrow(\uparrow\downarrow-\downarrow\uparrow) \\
+\; & \frac{1}{12}(2uudd+2dduu-udud-uddu-duud-dudu)\bar{s} \\
& \otimes(2\uparrow\uparrow\downarrow-\uparrow\downarrow\uparrow-\downarrow\uparrow\uparrow)(\uparrow\downarrow-\downarrow\uparrow)\Big]\,,
\end{aligned} \tag{4.7}$$

and

$$\begin{aligned}
|(8,1/2)(8,1)\rangle_{(\overline{10},1/2)} \;=\; & \frac{1}{\sqrt{2}}\Big[\frac{1}{2}(ud-du)(ud-du)\bar{s} \\
& \otimes\Big\{\frac{1}{\sqrt{3}}(\uparrow\downarrow-\downarrow\uparrow)\downarrow\uparrow\uparrow-\frac{1}{\sqrt{12}}(\uparrow\downarrow-\downarrow\uparrow)\uparrow(\uparrow\downarrow+\downarrow\uparrow)\Big\} \\
+\; & \frac{1}{\sqrt{12}}(2uudd+2dduu-udud-uddu-duud-dudu)\bar{s} \\
& \otimes\Big\{\frac{1}{3}(\uparrow\downarrow\downarrow+\downarrow\uparrow\downarrow-2\downarrow\downarrow\uparrow)\uparrow\uparrow \\
& -\frac{1}{6}(2\uparrow\uparrow\downarrow-\uparrow\downarrow\uparrow-\downarrow\uparrow\uparrow)(\uparrow\downarrow+\downarrow\uparrow)\Big\}\Big]\,.
\end{aligned} \tag{4.8}$$

These are sufficient to show $a'' = -1/2$ and $b'' = -\sqrt{3}/2$, using a sign convention consistent with our previous decomposition.

The CO wave function includes two possibilities. Either the orbital wave function is totally symmetric, $|CO\rangle_1$, or it has mixed symmetry, $|CO\rangle_2$, and the full wave function is

$$|CO\rangle = |CO\rangle_1 + |CO\rangle_2 \,. \tag{4.9}$$

For the totally symmetric orbital part, one has

$$\begin{aligned} |CO\rangle_1 &= \frac{1}{\sqrt{18}}\{\epsilon_{ijk}C^iC^jC^k\}\{C^l\bar{C}_l\}\otimes \\ &\left\{a'''(SSSPS) + b'''\frac{1}{\sqrt{3}}(SSP+SPS+PSS)SS\right\}, \end{aligned} \tag{4.10}$$

where we note that the P-state quark can be in either the q^3 or the $q\bar{q}$ part, and that the color wave function for the q^3 part is totally antisymmetric. The second possibility is that the q^3 orbital wave function has mixed symmetry and includes the P-state quark. The mixed symmetry orbital wave function may be either symmetric ($\mathrm{M_S}$) or antisymmetric ($\mathrm{M_A}$) under interchange of the first two quarks. These states combine with color 8_S or 8_A states as $[(\mathrm{M_S},8_A)-(\mathrm{M_A},8_S)]/\sqrt{2}$, to have a fully antisymmetric q^3 CO wave function. In this case the $q\bar{q}$ must be a color octet and its orbital part is symmetric. Thus,

$$\begin{aligned} |CO\rangle_2 &= \frac{c'''}{\sqrt{2}}\Bigg[\frac{1}{\sqrt{2}}(SP-PS)SSS \\ &\quad \frac{1}{4\sqrt{3}}\Big\{(C^iR+RC^i)(GB-BG)+(C^iG+GC^i)(BR-RB) \\ &\qquad +(C^iB+BC^i)(RG-GR)\Big\}\bar{C}_i \\ &\quad \otimes\Big\{\frac{1}{\sqrt{6}}(SP+PS)SSS-\sqrt{\frac{2}{3}}SSPSS\Big\} \\ &\quad \frac{1}{12}\{2(GB-BG)C^iR+2(BR-RB)C^iG+2(RG-GR)C^iB \\ &\qquad +\epsilon^{ijk}\epsilon_{jlm}\epsilon_{krs}C^lC^mC^rC^s\Big\}\bar{C}_i\Bigg]. \end{aligned} \tag{4.11}$$

The above wave function is antisymmetric by construction under the interchange of the first three quarks. The coefficients a''', b''', and c''' are found to be $1/2$, $-1/\sqrt{12}$, and $\sqrt{2/3}$, respectively, by antisymmetrizing on the first and fourth quarks.

4.3 Narrow Width

A narrow Θ^+ width can be understood if the overlap of the color-flavor-spin-orbital wave function with an NK final state is numerically small. The relevant piece of the FS wave function is $|(8,1/2)(8,0)\rangle$, which has coefficient $a'' = -1/2$. The relevant piece of the CO wave function has both the q^3 and $q\bar{q}$ in their relative ground states and has each of them separately color singlet. Furthermore, the terms of interest in the orbital wave function are totally symmetric in their q^3 and $q\bar{q}$ parts separately. These terms may be read from,

$$\begin{aligned} & \frac{a'''}{\sqrt{2}}(SSS)\left\{\frac{1}{\sqrt{2}}(PS+SP)+\frac{1}{\sqrt{2}}(PS-SP)\right\} \\ + \; & b'''\frac{1}{\sqrt{3}}(SSP+SPS+PSS)SS\,. \end{aligned} \tag{4.12}$$

The totally symmetric orbital wave functions with a P-state included correspond to a ground state baryon or meson with center-of-mass motion. From the previous section we know $a''' = 1/2$ and $b''' = -1/\sqrt{12}$. Hence the total probability of the Θ^+ overlap with NK is:

$$c_+ = \left(a''a'''/\sqrt{2}\right)^2 + (a''b''')^2 = \frac{5}{96}\,, \tag{4.13}$$

which implicitly includes a sum over z-component spin projections. This is interestingly small. The Θ^+ width for a positive (Γ_+) or negative (Γ_-) parity state is

$$\begin{aligned} \Gamma_\pm \;&=\; c_\pm\, g_\pm^2 \cdot \frac{M}{16\pi}\left[(1-\frac{(m+\mu)^2}{M^2})(1-\frac{(m-\mu)^2}{M^2})\right]^{1/2} \\ &\times\; \left[(1\mp\frac{m}{M})^2-\frac{\mu^2}{M^2}\right]\,, \end{aligned} \tag{4.14}$$

where M, m and μ are the masses of the Θ^+, the final state baryon and the meson, respectively, $c_\pm$ is the dimensionless spin-flavor-color-orbital overlap factor ($c_+ = 5/96$, or $c_- = 1/4$ from Ref. [65]), and $g_\pm$ is an effective meson-baryon coupling constant, $\mathcal{L}_{eff}(c_\pm = 1) = g_-\bar{N}K^\dagger\Theta^+$ or $ig_+\bar{N}\gamma^5K^\dagger\Theta^+$. Applying the rules of naive dimensional

analysis (NDA) [98], one estimates that $g_\pm \sim 4\pi$, up to order one factors. One then finds

$$\Gamma_+ \approx 4.4 \text{ MeV while } \Gamma_- \approx 1.1 \text{ GeV}. \tag{4.15}$$

In the effective theory approach, effects associated with long-distance dynamics are subsumed in the values of the couplings $g_\pm$. For example, an explicit computation of quark wave function overlaps in baryons with both S- and P-wave constituents could lead to a smaller estimate for g_+. However, the precise outcome is strongly model dependent and we do not pursue this issue further. Our result implies that a positive parity Θ^+ is narrow, independent of these uncertainties.

It has been noted [66] that the correlated diquark state advocated in Ref. [43] has a small overlap with the NK state, even if one just considers the color-flavor-spin wave function. However, the q^4 part of the correlated diquark state presented in [43] is not perfectly antisymmetric. The state is a good approximation to a Fermi-Dirac allowed state only to the extent that the diquarks are significantly more compact than the overall state. The significant likelihood that the diquarks are comparable in size to the entire pentaquark is reason for concentrating on a consistent, antisymmetrized wave function. (We can nonetheless report for the correlated diquark model that inclusion of the orbital wave function reduces the Θ^+ overlap with NK from the Jennings-Maltman [66] color-flavor-spin result of $1/24$ to a remarkably small $5/576$.)

4.4 Conclusions

We have presented an explicit framework in which the width of a positive parity Θ^+ is narrow. We find that the spin-flavor-color-orbital overlap probability for decays to kinematically allowed final states is $5/96$. By comparison, the same overlap probability for the negative parity case is $1/4$, as was shown in Ref. [65]. Without any incalculable dynamical suppression (that could render g_- substantially less than g_+ above), one may

infer that a negative parity pentaquark state, if it exists, is significantly broader than its positive parity cousin. Aside from its NK component, the even parity Θ^+ wave function overlaps with other color-singlet-color-singlet baryon-meson states that are together heavier than the Θ^+, and with color-octet-color-octet baryon-meson states. Hence, even though the decay proceeds via a fall-apart mode, the amplitude to kinematically allowed baryon-meson states is small.

CHAPTER 5

Photoproduction of the Θ^+ resonance on the nucleon in a Regge model

5.1 Introduction

It is quite obvious from discussions in the previous chapter that theoretically, QCD does not prohibit the existence of pentaquark states. If there are any prejudices, we should expect the existence of the exotic states such as dibaryons, dimesons, glueballs and pentaquarks. For the pentaquark, the problems are where to look for the states and how to distinguish them from the ordinary baryon resonances. Also if the states are very wide, the search might be futile since we will not be able to distinguish the resonances from the background. After years of searches with no results, the community seemed to give up when PDG after 1986 [99] dropped the section on searches for pentaquarks. Recent interest for pentaquarks was sparked again after the announcement from SPring-8 experiment [1]. The experiments were conducted with the guidance of the chiral quark soliton model estimate by Diakonov *et. al.* [51], which predicted the existence of a narrow baryon resonance with strangeness ($S = 1$) at mass around 1530 MeV. Criticism for this

paper can be found in [61, 62]. The paper also predicted that the resonance has spin 1/2 and positive parity as predicted by subsequent chiral soliton model works [42, 44, 48, 67]. A naive constituent quark model will give a negative parity state [65], even though it is also possible to have a positive parity state in a quark model if one introduces a P-wave in the spatial wavefunction [31, 43, 53]. As for the spin of the Θ^+, all theory paper to our knowledge predicts 1/2 and consider spin-3/2 to be a heavier excitation state, see *e.g.* Ref. [93].

The most puzzling issues from the theoretical point of view right now is the narrow width of the Θ^+. The chiral quark soliton model work by Diakonov *et. al* [51] did naturally predict an anomalously narrow width for the Θ^+. Some attempts also have been made in constituent quark models to explain the narrow width, *e.g.* [31, 39, 100]. For an early review on these theoretical issues see [66].

Clearly, to address the issues mentioned above, *i.e.* existence, spin-parity assignment and width of the pentaquark, more dedicated experiments are needed. Production mechanisms are a key aspect in this study since it has been argued that certain processes will not be effective to produce the pentaquark. Many efforts have been made in the past to study the θ^+ photo- and electroproduction processes [15, 16, 17, 71, 101, 102, 103, 104, 105, 106, 107, 108, 109, 110, 111], even though most of the cross section predictions have been ruled out by the recent JLAB g10 and g11 experiments [14, 112].

In this chapter we make another effort to study the photoproduction mechanism for the Θ^+ using a Regge model, which has been found to successfully describe the main features of $K\Lambda$ and $K\Sigma$ photoproduction on the nucleon at *c.m.* energies above 2 GeV [113, 114, 115]. In section II we discuss the theory of Regge exchange mechanism. We also discuss the relation of the width to the photoproduction cross section of the Θ^+. In view of upcoming high resolution experiments [116], such a link is needed to translate quantitatively an upper limit on the photoproduction cross section into an upper bound on the Θ^+ width. In section III we present the results of our calculation for the

Θ^+ photoproduction cross sections. We also study photon asymmetry and decay angular distribution of the Θ^+ photoproduction. We close with our conclusion in section IV.

5.2 Regge model

At sufficiently high energies, above the nucleon resonance region, strangeness photo- and electroproduction reactions (e.g. $\gamma p \to K^+\Lambda, K^+\Sigma$) at forward angles are dominated by K and K^* Regge exchanges as has been proposed long time ago in Ref. [117], and studied in detail in view of numerous recent strangeness photo- and electroproduction data in Refs. [113, 114, 115]. It was found in those works that the simple Regge model for open strangeness electromagnetic production reactions in terms of K and K^* exchanges provides an economical description and simple explanation of the forward angle data for total *c.m.* energy $W > 2$ GeV. It surprisingly reproduces the gross features of the data, even for $W < 2$ GeV, hinting that a sort of reggeon-resonance duality is at work.

In this work, our aim is to extend this model to the description of the process

$$\gamma(q) + N(p_N) \longrightarrow K(p_K) + \Theta^+(p_\Theta). \tag{5.1}$$

The Mandelstam variables for this process are given by $s \equiv (p_N+q)^2$, $t \equiv (q-p_K)^2$, and $u \equiv (q-p_\Theta)^2$, satisfying $s+t+u = M_N^2+m_K^2+M_\Theta^2$, with M_N the nucleon mass, m_K the kaon mass, and M_Θ the mass of the Θ^+. In this work we take as input value the mass of the Θ^+, $M_\Theta = 1.54$ GeV, consistent with the experiments of Refs. [1, 2, 3, 4, 5, 6, 7, 9, 10]. Our description of the reaction (5.1) in terms of reggeized K and K^* t-channel exchanges is aimed at the region of large s ($W = \sqrt{s} > 2$ GeV) and small $-t$ ($-t << s$). We discuss subsequently the t-channel K and K^* Regge exchange processes for reaction (5.1) as is shown in Fig. 5.1.

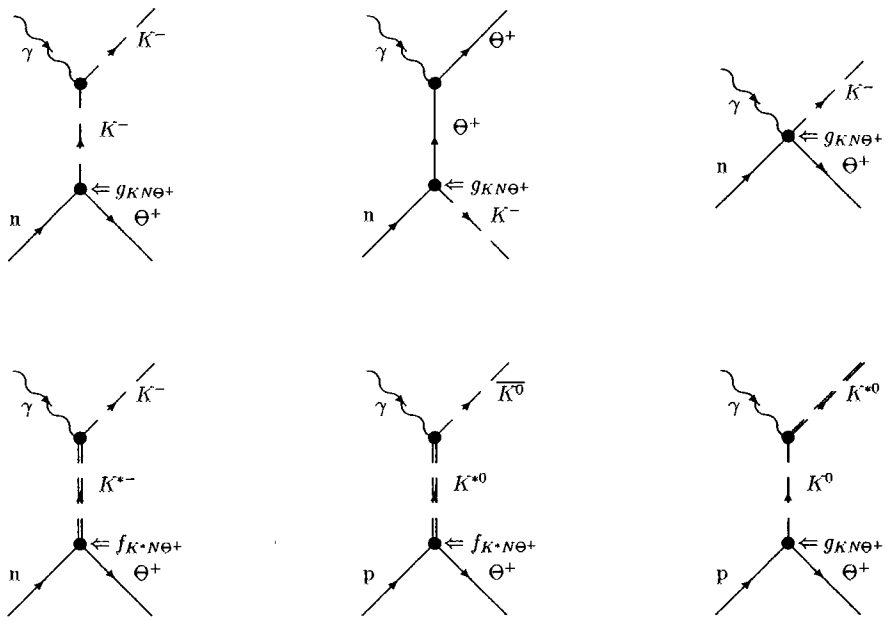

FIG. 5.1: The different Regge exchange contributions considered to describe the photoproduction reactions with Θ^+ final state on a nucleon.

5.2.1 K Regge exchange

Spin-1/2 Θ^+ Amplitude

The construction of the reggeized amplitude for the charged K-exchange process to the $\gamma n \to K^-\Theta^+$ reaction, as shown in Fig. 5.1, amounts to replace the usual Feynman pole propagator for the kaon by a 'Regge propagator' function, depending on both s and t, i.e. $\mathcal{P}^K_{Regge}(s,t)$ as follows :

$$\frac{1}{t-m_K^2} \Longrightarrow \mathcal{P}^K_{Regge}(s,t) = \left(\frac{s}{s_0}\right)^{\alpha_K(t)} \frac{\pi\alpha'_K}{\sin(\pi\alpha_K(t))} \frac{\mathcal{S}_K + e^{-i\pi\alpha_K(t)}}{2} \frac{1}{\Gamma(1+\alpha_K(t))} . \tag{5.2}$$

Such a Regge propagator function effectively takes into account the exchange of high-spin particles (in the t-channel) which lie on the K Regge trajectory $\alpha_K(t) = \alpha^0_K + \alpha'_K \cdot t$. For the K, we use a standard linear trajectory in Eq. (5.2) :

$$\alpha_K(t) = 0.7\,(t - m_K^2)\,, \tag{5.3}$$

which was previously used in the analysis of strangeness photoproduction reactions at high energies [113]. Furthermore, in Eq. (5.2), the mass scale s_0 is typically taken as $s_0 = 1$ GeV^2, and $\mathcal{S} = \pm 1$ is the signature of the trajectory [118]. For the kaon trajectory, the states with $J^P = 0^-, 2^-, 4^-, ...$ correspond with $\mathcal{S} = +1$, whereas the states with $J^P = 1^+, 3^+, 5^+, ...$ correspond with $\mathcal{S} = -1$. The gamma function $\Gamma(1 + \alpha(t))$ suppresses poles of the propagator in the unphysical region. As is well known from Regge theory [118], trajectories can be either non-degenerate or degenerate. A degenerate trajectory is obtained by adding or subtracting the two non-degenerate trajectories with the two opposite signatures. As can be seen from the numerator of Eq. (5.2), this leads to trajectories with either a rotating ($e^{-i\pi\alpha(t)}$) or a constant (1) phase. In line with the finding of Ref. [113] for the charged K trajectory entering in strangeness photoproduction processes, we use the rotating phase in the following. This corresponds with the so-called strong degeneracy assumption [118] in Regge terminology, and amounts to replace in Eq. (5.2) the factor $(\mathcal{S}_K + e^{-i\pi\alpha_K(t)})/2$ by $e^{-i\pi\alpha_K(t)}$. One can easily verify that the Regge propagator reduces to the Feynman propagator $1/(t - m_K^2)$ if one approaches the first pole on a trajectory (i.e. when taking $t \to m_K^2$ in Eq. (5.2)).

In order to calculate the K Regge exchange contribution to the Θ^+ photoproduction amplitude as shown in Fig. 5.1, we have to specify the $KN\Theta^+$ vertex function. We subsequently study this vertex for the cases of spin and parity assignments $1/2^\pm$ and $3/2^\pm$ of the Θ^+ resonance.

- $J^P = \frac{1}{2}^+$

  For the spin parity assignment of the Θ^+ resonance given by $J^P = \frac{1}{2}^+$, the $KN\Theta^+$ vertex can be written as :

$$\mathcal{L}_{KN\Theta} = i\, g_{KN\Theta} \left(K^\dagger \bar{\Theta} \gamma_5 N + \bar{N} \gamma_5 \Theta K \right) , \tag{5.4}$$

  where K and N are the kaon and nucleon isospin doublet fields respectively, and

where Θ is the Θ^+ isosinglet field. The Lagrangian of Eq. (5.4) corresponds with the Θ^+ being a p-wave resonance in the KN system. With this Lagrangian, the decay width $\Gamma_{\Theta\to KN}$ is given by :

$$\Gamma_{\Theta\to KN} = \frac{g^2_{KN\Theta}}{2\pi}\frac{|\bar{p}_K|}{M_\Theta}\left(\sqrt{\bar{p}_K^2 + M_N^2} - M_N\right), \tag{5.5}$$

where $|\bar{p}_K| \simeq 0.267$ GeV is the kaon momentum in the rest frame of the Θ^+. To extract a value for $g_{KN\Theta}$, we need the experimental information of the width $\Gamma_{\Theta\to KN}$, which is not known precisely at this moment but whose measurement is the subject of several planned dedicated experiments, e.g. Refs. [116]. To provide numerical estimates in this work, we will use $\Gamma_{\Theta\to KN}$ = 1 MeV as the value for the width, which is consistent with the upper limit for the width derived from elastic KN scattering [119]. Evaluating Eq. (5.5) with $\Gamma_{\Theta\to KN}$ = 1 MeV, we then extract the value $g_{KN\Theta} \simeq 1.056$, which will be used in all of the following estimates for $J^P = \frac{1}{2}^+$ Θ^+.

- $J^P = \frac{1}{2}^-$

For the spin parity assignment of the Θ^+ resonance given by $J^P = \frac{1}{2}^-$, the $KN\Theta^+$ vertex can be written as :

$$\mathcal{L}_{KN\Theta} = g_{KN\Theta}\left(K^\dagger\bar{\Theta}N + \bar{N}\Theta K\right), \tag{5.6}$$

which corresponds with the Θ^+ being a s-wave resonance in the KN system. In this case, the decay width $\Gamma_{\Theta\to KN}$ is given by :

$$\Gamma_{\Theta\to KN} = \frac{g^2_{KN\Theta}}{2\pi}\frac{|\bar{p}_K|}{M_\Theta}\left(\sqrt{\bar{p}_K^2 + M_N^2} + M_N\right). \tag{5.7}$$

Using $\Gamma_{\Theta\to KN}$ = 1 MeV as the value for the width, we obtain $g_{KN\Theta} \simeq 0.1406$, which will be used in the following estimates for $J^P = \frac{1}{2}^-$ Θ^+.

Having specified the Regge propagator and $KN\Theta$ vertex function, we can construct the gauge invariant reggeized charged K-exchange amplitude for the $\gamma n \to K^- \Theta^+$ process for the spin-1/2 Θ^+ as :

$$\begin{aligned}
&\mathcal{M}_K\left(\gamma n \to K^- \Theta^+ : J^P_\Theta = \frac{1}{2}^+\right) = \\
&\quad e\, g_{KN\Theta} \cdot \mathcal{P}^K_{Regge}(s,t) \cdot \varepsilon_\mu(q,\lambda) \\
&\quad \times \Big[F_K(t) \cdot (2p_K - q)^\mu \cdot \bar{\Theta}\gamma^5 N \\
&\qquad - F_\Theta(u) \cdot (t - m_K^2) \cdot \bar{\Theta}\gamma^\mu \frac{(\gamma \cdot p_u + M_\Theta)}{u - M_\Theta^2}\gamma^5 N \\
&\qquad + 2p_K^\mu \cdot (\hat{F}(s,t,u) - F_K(t)) \cdot \bar{\Theta}\gamma^5 N \\
&\qquad - \left(\frac{t - m_K^2}{u - m_\Theta^2}\right) \cdot 2p_\Theta^\mu \cdot \{\hat{F}(s,t,u) - F_\Theta(u)\} \cdot \bar{\Theta}\gamma^5 N\Big] ,
\end{aligned} \tag{5.8}$$

$$\begin{aligned}
&\mathcal{M}_K\left(\gamma n \to K^- \Theta^+ : J^P_\Theta = \frac{1}{2}^-\right) = \\
&\quad (-i)\, e\, g_{KN\Theta} \cdot \mathcal{P}^K_{Regge}(s,t) \cdot \varepsilon_\mu(q,\lambda) \\
&\quad \times \Big[F_K(t) \cdot (2p_K - q)^\mu \cdot \bar{\Theta} N \\
&\qquad - F_\Theta(u) \cdot (t - m_K^2) \cdot \bar{\Theta}\gamma^\mu \frac{(\gamma \cdot p_u + M_\Theta)}{u - M_\Theta^2} N \\
&\qquad + 2p_K^\mu \cdot (\hat{F}(s,t,u) - F_K(t)) \cdot \bar{\Theta} N \\
&\qquad - \left(\frac{t - m_K^2}{u - m_\Theta^2}\right) \cdot 2p_\Theta^\mu \cdot \{\hat{F}(s,t,u) - F_\Theta(u)\} \cdot \bar{\Theta} N\Big] ,
\end{aligned} \tag{5.9}$$

where $\varepsilon_\mu(q,\lambda)$ is the photon polarization vector with photon polarization $\lambda = \pm 1$. To evaluate the Regge vertex functions (Regge residues) away from the pole position, we include the form factors $F_K(t)$, $F_\Theta(u)$, and $\hat{F}$ in the amplitude formulas above. In our calculations, we choose monopole forms for F_K and F_u :

$$F_K(t) = \left(1 + \frac{-t + m_K^2}{\Lambda^2}\right)^{-1} , \tag{5.10}$$

$$F_\Theta(u) = \left(1 + \frac{-u + M_\Theta^2}{\Lambda^2}\right)^{-1} . \tag{5.11}$$

For the cut-off Λ, we choose a typical hadronic scale of $\Lambda = 1$ GeV. In Eqs. (5.9,5.9), the terms proportional to F_K are the t-channel process (top left diagram in Fig. 5.1),

whereas the terms proportional to F_u originate from the process with the Θ^+ in the u-channel (top middle diagram in Fig. 5.1). In the Regge approach, this gauge restoring term is reggeized in the same way as for the t-channel process, see e.g. Refs. [120, 113]. In particular, one notices that at the K pole, the pre-factors $(t - m_K^2)$ in the second terms of Eqs. (5.9,5.9) exactly compensate the Regge function $\mathcal{P}^K_{Regge}$, reducing these contributions to standard u-channel pole terms. For the $\gamma p \to K^+(\Lambda, \Sigma)$ reactions, it has been shown in Ref. [114, 115] that this gauge invariant reggeization procedure (for the case where the form factors are absent), by restoring the gauge invariance of the t-channel charged kaon exchange process through proper reggeization of the s-channel (for K^+) or u-channel (for K^-) processes, is a key to reproduce several strangeness photo- and electroproduction observables. The third and fourth terms which contain $\hat{F}$ are contact terms which are required by gauge invariance when including form factors. The only restriction we applied to these terms is they should not have poles at $t = m_K^2$ and $u = m_\Theta^2$. With this restriction, we can choose the form :

$$\hat{F}(s,t,u) = F_K(t) + F_\Theta(u) - F_K(t) \cdot F_\Theta(u). \tag{5.12}$$

Note that $\hat{F} - F_K(t)$ is proportional to $(t - m_K^2)$, whereas $\hat{F} - F_\Theta(u)$ is proportional to $(u - M_\Theta^2)$, thus canceling the poles in the contact terms.

Spin-3/2 Θ^+ Amplitude

- $J^P = \frac{3}{2}^+$

  For the spin parity assignment of the Θ^+ resonance given by $J^P = \frac{3}{2}^+$, the $KN\Theta^+$ vertex can be written as :

$$\mathcal{L}_{KN\Theta} = \frac{g_{KN\Theta}}{m_K} \left\{ \bar{\Theta}^\alpha g_{\alpha\beta} N \left(\partial^\beta K\right) + \bar{N} \Theta^\alpha g_{\alpha\beta} \left(\partial^\beta K^\dagger\right) \right\} . \tag{5.13}$$

  The Lagrangian of Eq. (5.13) corresponds with the Θ^+ being a p-wave resonance in

the KN system. In this case, the decay width $\Gamma_{\Theta\to KN}$ is given by :

$$\Gamma_{\Theta\to KN} = \frac{g^2_{KN\Theta}}{2\pi}\frac{|\vec{p}_K|}{M_\Theta}\frac{|\vec{p}_K|^2}{3m^2_K}\left(\sqrt{\vec{p}^2_K+M^2_N}+M_N\right). \quad (5.14)$$

Again using $\Gamma_{\Theta\to KN}$ = 1 MeV as value for the width, we obtain $g_{KN\Theta}\simeq 0.4741$, which will be used in the following estimates for $J^P=\frac{3}{2}^+$ Θ^+.

- $J^P=\frac{3}{2}^-$

For the spin parity assignment of the Θ^+ resonance given by $J^P=\frac{3}{2}^-$, the $KN\Theta^+$ vertex can be written as :

$$\mathcal{L}_{KN\Theta} = \frac{g_{KN\Theta}}{m_K}\left\{\bar{\Theta}^\alpha\gamma_5 N g_{\alpha\beta}\left(\partial^\beta K\right)+\bar{N}\gamma_5\Theta^\alpha g_{\alpha\beta}\left(\partial^\beta K^\dagger\right)\right\}. \quad (5.15)$$

The Lagrangian of Eq. (5.15) corresponds with the Θ^+ being a d-wave resonance in the KN system. In this case, the decay width $\Gamma_{\Theta\to KN}$ is given by :

$$\Gamma_{\Theta\to KN} = \frac{g^2_{KN\Theta}}{2\pi}\frac{|\vec{p}_K|}{M_\Theta}\frac{|\vec{p}_K|^2}{3m^2_K}\left(\sqrt{\vec{p}^2_K+M^2_N}-M_N\right). \quad (5.16)$$

Finally, using $\Gamma_{\Theta\to KN}$ = 1 MeV as value for the width, we obtain $g_{KN\Theta}\simeq 3.558$, which will be used in the following estimates for $J^P=\frac{3}{2}^-$ Θ^+.

Having specified the $KN\Theta$ vertex function for spin-3/2, we can construct the gauge invariant reggeized charged K-exchange amplitude for the $\gamma n\to K^-\Theta^+$ process for the $3/2^-$ Θ^+ as :

$$\mathcal{M}_K\left(\gamma n \to K^- \Theta^+ : J^P_\Theta = \frac{3}{2}^+\right) =$$
$$\frac{i\,e\,g_{KN\Theta}}{m_K} \cdot \mathcal{P}^K_{Regge}(s,t) \cdot \varepsilon_\mu(q,\lambda)$$
$$\times \Big[F_K(t) \cdot (2p_K - q)^\mu \cdot (p_K - q)^\alpha \cdot \bar{\Theta}_\alpha N$$
$$- F_\Theta(u) \cdot (t - m_K^2) \cdot \bar{\Theta}_\alpha \gamma^{\alpha\beta\mu} \frac{(\gamma \cdot p_u + M_\Theta)}{u - M_\Theta^2}$$
$$\cdot S_{\beta\nu} \cdot \gamma^{\nu\sigma\rho} \frac{(p_K)_\sigma \cdot (p_u)_\rho}{M_\Theta^2} N$$
$$+ (t - m_K^2) \cdot \bar{\Theta}_\alpha \gamma^{\alpha\mu\nu} \frac{(F_\Theta(u) \cdot p_K + F_K(t) \cdot p_\Theta)_\nu}{M_\Theta} N$$
$$+ 2p_K^\mu \cdot (\hat{F}(s,t,u) - F_K(t)) \cdot p_K^\alpha \cdot \bar{\Theta}\, N$$
$$- \left(\frac{t - m_K^2}{u - m_\Theta^2}\right) \cdot 2p_\Theta^\mu \cdot \{\hat{F}(s,t,u) - F_\Theta(u)\} \cdot p_K^\alpha \cdot \bar{\Theta}\, N\Big], \quad (5.17)$$

$$\mathcal{M}_K\left(\gamma n \to K^- \Theta^+ : J^P_\Theta = \frac{3}{2}^-\right) =$$
$$\frac{-e\,g_{KN\Theta}}{m_K} \cdot \mathcal{P}^K_{Regge}(s,t) \cdot \varepsilon_\mu(q,\lambda)$$
$$\times \Big[F_K(t) \cdot (2p_K - q)^\mu \cdot (p_K - q)^\alpha \cdot \bar{\Theta}_\alpha \gamma^5 N$$
$$- F_\Theta(u) \cdot (t - m_K^2) \cdot \bar{\Theta}_\alpha \gamma^{\alpha\beta\mu} \frac{(\gamma \cdot p_u + M_\Theta)}{u - M_\Theta^2}$$
$$\cdot S_{\beta\nu} \cdot \gamma^{\nu\sigma\rho} \frac{(p_K)_\sigma \cdot (p_u)_\rho}{M_\Theta^2} \gamma^5 N$$
$$+ (t - m_K^2) \cdot \bar{\Theta}_\alpha \gamma^{\alpha\mu\nu} \frac{(F_\Theta(u) \cdot p_K + F_K(t) \cdot p_\Theta)_\nu}{M_\Theta} \gamma^5 N$$
$$+ 2p_K^\mu \cdot (\hat{F}(s,t,u) - F_K(t)) \cdot p_K^\alpha \cdot \bar{\Theta}\, \gamma^5 N$$
$$- \left(\frac{t - m_K^2}{u - m_\Theta^2}\right) \cdot 2p_\Theta^\mu \cdot \{\hat{F}(s,t,u) - F_\Theta(u)\} \cdot p_K^\alpha \cdot \bar{\Theta}\, \gamma^5 N\Big], \quad (5.18)$$

with

$$S_{\beta\nu} = g_{\beta\nu} - \frac{\gamma_\beta \gamma_\nu}{3} - \frac{(\gamma_\beta (p_u)_\nu - \gamma_\nu (p_u)_\beta)}{3M_\Theta} - \frac{2((p_u)_\beta (p_u)_\nu)}{3M_\Theta}.$$

Similar to the spin-1/2 case, the form factors $F_K(t)$ and $F_\Theta(u)$ have to be added to take into account the change of coupling constant $g_{KN\Theta}$ away from the pole position. In the calculation, we choose the same forms of $F_K(t)$ and $F_\Theta(u)$ for spin-3/2 as for the spin-1/2 case. For the spin-3/2 case we have to add the third, fourth and fifth terms in Eqs. (5.18,5.18), which originate from the contact diagrams to the t- and u-channel process to preserve gauge invariant in the amplitude. In the Regge approach, this gauge restoring term is reggeized in the same way as for the t-channel process, as discussed before for the spin-1/2 case. We also choose the $\hat{F}(s,t,u)$ to have the same form as for the spin-1/2 case.

5.2.2 K^* Regge exchange

We next consider the $K^*(892)$ exchange processes to both the $\gamma n \to K^-\Theta^+$ and $\gamma p \to \bar{K}^0\Theta^+$ reactions as shown in Fig. 5.1. Note that for the $\gamma p \to \bar{K}^0\Theta^+$ reaction, K exchange is not possible as the real photon does not couple to the neutral kaon. Therefore, we expect K^* exchange to be the dominant t-channel mechanism for the $\gamma p \to \bar{K}^0\Theta^+$ reaction.

The construction of the reggeized amplitude for the K^*-exchange processes, amounts to replace the K^* pole by a 'Regge propagator' function $\mathcal{P}^{K^*}_{Regge}(s,t)$:

$$\frac{1}{t-m^2_{K^*}} \Longrightarrow \mathcal{P}^{K^*}_{Regge} = \left(\frac{s}{s_0}\right)^{\alpha_{K^*}(t)-1} \frac{\pi\alpha'_{K^*}}{\sin(\pi\alpha_{K^*}(t))} \frac{\mathcal{S}^*_K + e^{-i\pi\alpha_{K^*}(t)}}{2} \frac{1}{\Gamma(\alpha_{K^*}(t))}\,, \tag{5.19}$$

For the $K^*(892)$, we use a standard linear trajectory :

$$\alpha_{K^*}(t) = 0.25 + \alpha'_{K^*}\, t\,, \tag{5.20}$$

where $\alpha'_{K^*} = 0.83$ GeV^{-2}. Furthermore, we also consider a degenerate trajectory for K^* leading to a Regge propagator with rotating phase in Eq. (5.19), in line with our previous findings in the analysis of strangeness photoproduction reactions at high energies [113].

To evaluate the K^* processes in Fig. 5.1, we next have to specify the $K^*N\Theta^+$ vertex function. If the spin parity assignment of the Θ^+ resonance is given by $J^P = \frac{1}{2}^+$, the $K^*N\Theta^+$ vertex can be written as :

$$\mathcal{L}_{K^*N\Theta} = f_{K^*N\Theta}\,\bar{\Theta}\left[\frac{i\,\sigma_{\mu\nu}\,p^{\nu}_{K^*}}{M_N + M_\Theta}\right] N \cdot V^{\mu}(p_{K^*}) + \text{h.c.}\,, \tag{5.21}$$

where $V^{\mu}(p_{K^*})$ is the polarization vector of the K^* meson. If the spin parity assignment of the Θ^+ resonance is given by $J^P = \frac{1}{2}^-$, the $K^*N\Theta^+$ vertex is given by :

$$\mathcal{L}_{K^*N\Theta} = -i\,f_{K^*N\Theta}\,\bar{\Theta}\left[\frac{i\,\sigma_{\mu\nu}\,p^{\nu}_{K^*}}{M_N + M_\Theta}\right]\gamma_5\, N \cdot V^{\mu}(p_{K^*}) + \text{h.c.}\,. \tag{5.22}$$

Using $SU(3)$ symmetry for the vector meson couplings within the baryon octet and between the baryon octet and antidecuplet, one can express :

$$g_{\rho^0 pp} + f_{\rho^0 pp} = \frac{7}{10}\left(V_0 + \frac{1}{2}V_1\right) + \frac{1}{20}V_2, \tag{5.23}$$

$$g_{\omega pp} + f_{\omega pp} = \frac{1}{10}\left(V_0 + \frac{1}{2}V_1\right) + \frac{23}{20}V_2, \tag{5.24}$$

$$g_{\phi pp} + f_{\phi pp} = -\frac{1}{10}\left(V_0 + \frac{1}{2}V_1\right) + \frac{7}{20}V_2, \tag{5.25}$$

$$f_{K^{*0}\Theta^+ p} = \frac{3}{\sqrt{30}}\left(V_0 - V_1 - \frac{1}{2}V_2\right), \tag{5.26}$$

where $g_{VNN}(f_{VNN})$ are the vector (tensor) coupling constants respectively. First we use the fact that $g_{\phi pp} + f_{\phi pp} \simeq 0$ [121], and solve for V_2 in Eq. (5.25). Substituting this into Eqs. (5.23) and (5.26), we can express the $K^*N\Theta$ coupling as :

$$f_{K^{*0}p\Theta^+} = (g_{\rho^0 pp} + f_{\rho^0 pp})\,\frac{3\sqrt{3}}{\sqrt{10}}\,\frac{4/5 - r}{r+2}, \tag{5.27}$$

where r is defined as $r \equiv V_1/V_0$. By fixing the ratio r to its value obtained in the chiral quark soliton model [51] : $r \simeq 0.35$ and using the value $g_{\rho^0 pp} + f_{\rho^0 pp} \simeq 18.7$ [122], Eq. (5.27) then leads to the coupling $f_{K^*N\Theta} = \simeq 5.9$. Note that the value of $f_{K^{*0}p\Theta^+}$ is very sensitive to the value of the parameter r, as there is a strong cancellation of various contributions. The case of 1 MeV width of Θ^+ indicates that this cancellation can be very

deep. The above mentioned value obtained in the particular dynamical model is subjected to large theoretical uncertainties which result in big spread in values of the coupling constant. Here we assume that the parameter r is close to the value of its counterpart for the axial transitions which corresponds with a width of Θ^+ of about 1 MeV. This assumption yields :

$$f_{K^*N\Theta} \equiv f_{K^{*0}p\Theta^+} \simeq 1.1\,, \tag{5.28}$$

which will be used for the coupling constant entering in the vertices of Eqs. (5.21,5.22) for both parities of the Θ^+.

The reggeized K^* exchange amplitudes for both parities of the Θ^+ are then given by :

$$\begin{aligned}\mathcal{M}_{K^*}\left(\gamma p \to \bar{K}^0\Theta^+ : J^P_\Theta = \frac{1}{2}^+\right) &= i\,e\,f_{K^{*0}K^0\gamma}\,f_{K^*N\Theta}\cdot\mathcal{P}^{K^*}_{Regge}(s,t)\cdot\varepsilon^\mu(q,\lambda)\\ &\times\ \varepsilon_{\mu\nu\lambda\alpha}\,q^\nu\,(q-p_K)^\lambda\,\bar{\Theta}\left[\frac{i\,\sigma^{\alpha\beta}\,(q-p_K)_\beta}{M_N+M_\Theta}\right]N\,,\end{aligned} \tag{5.29}$$

$$\begin{aligned}\mathcal{M}_{K^*}\left(\gamma p \to \bar{K}^0\Theta^+ : J^P_\Theta = \frac{1}{2}^-\right) &= e\,f_{K^{*0}K^0\gamma}\,f_{K^*N\Theta}\cdot\mathcal{P}^{K^*}_{Regge}(s,t)\cdot\varepsilon^\mu(q,\lambda)\\ &\times\ \varepsilon_{\mu\nu\lambda\alpha}\,q^\nu\,(q-p_K)^\lambda\,\bar{\Theta}\left[\frac{i\,\sigma^{\alpha\beta}\,(q-p_K)_\beta}{M_N+M_\Theta}\right]\gamma_5\,N\,,\end{aligned} \tag{5.30}$$

and analogous formulas hold for the K^* contribution to the $\gamma n \to K^-\Theta^+$ reaction. In Eqs. (5.29,5.30), the electromagnetic coupling $f_{K^*K\gamma}$ can be extracted from the radiative decay widths $\Gamma_{K^{*0}\to K^0\gamma} = 0.117$ MeV, and $\Gamma_{K^{*-}\to K^-\gamma} = 0.05$ MeV, yielding [113] :

$$f_{K^{*0}K^0\gamma} = 1.28\ \text{GeV}^{-1}\,, \tag{5.31}$$

$$f_{K^{*-}K^-\gamma} = 0.84\ \text{GeV}^{-1}\,. \tag{5.32}$$

Note that the K^* t-channel exchange amplitudes of Eqs. (5.29,5.30) are gauge invariant by themselves.

5.3 Results

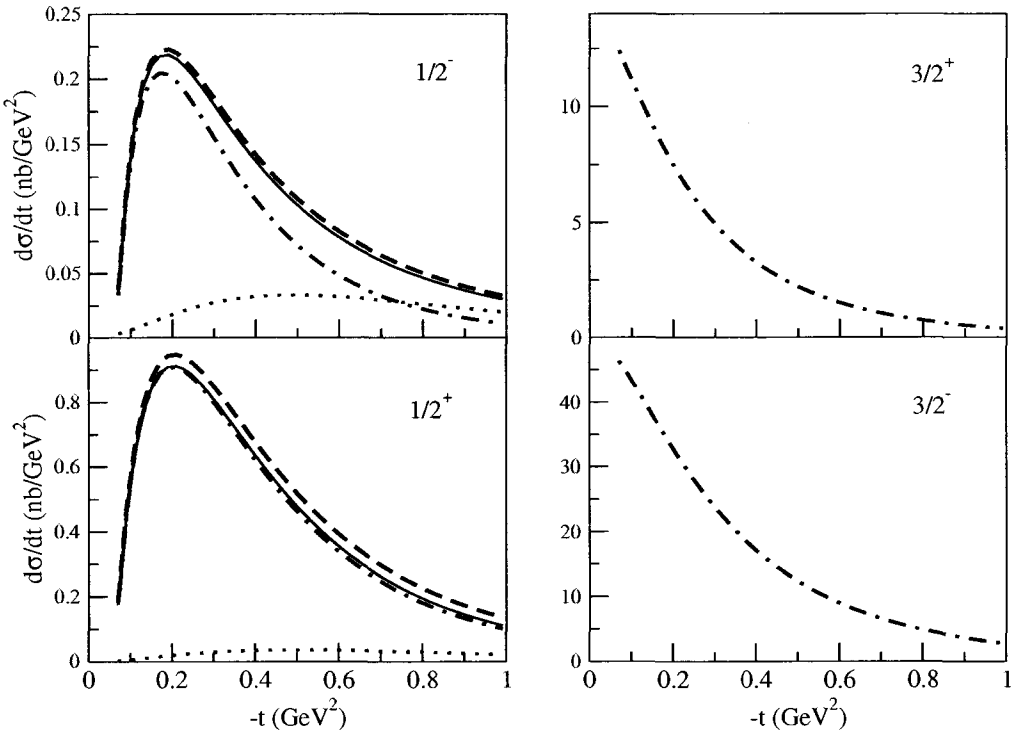

FIG. 5.2: Regge model predictions for the $\gamma n \to K^- \Theta^+$ cross section at $E_\gamma = 4$ GeV for different spin parity assignments of the Θ^+. Dashed-dotted curves : gauge invariant K Regge exchange; dotted curves : K^* Regge exchange (for the cases of $1/2^\pm$). To account for the range of uncertainty in the $K^*N\Theta$ coupling, we display the result for $K+K^*$ exchange for two values of the $K^*N\Theta$ coupling constant : $f_{K^*N\Theta} = +1.1$ (solid curves), and $f_{K^*N\Theta} = -1.1$ (dashed curves), corresponding with a width $\Gamma_{\Theta \to KN} = 1$ MeV.

In Fig. 5.2, we show our results for the differential cross section for the $\gamma n \to K^- \Theta^+$ reaction for the cases of spin-parity assignments $1/2^\pm$ and $3/2^\pm$ of the Θ^+. Comparing the cross sections for K Regge exchange for the cases of $J^P = 1/2^\pm$, one notices that the $KN\Theta$ coupling constant for the case of a negative parity Θ^+ is a factor 7 smaller than for the case of a positive parity Θ^+. If there were only t-channel K exchange, this would result in a ratio of about a factor 50 for the cross sections of positive parity compared to negative parity Θ^+ photoproduction for the case of a Θ^+ of $J = 1/2$. The cross section for $J^P_\Theta = 1/2^-$ gets enhanced though through the u-channel Θ^+ process and the contact diagrams, which are required to make the t-channel charged kaon exchange

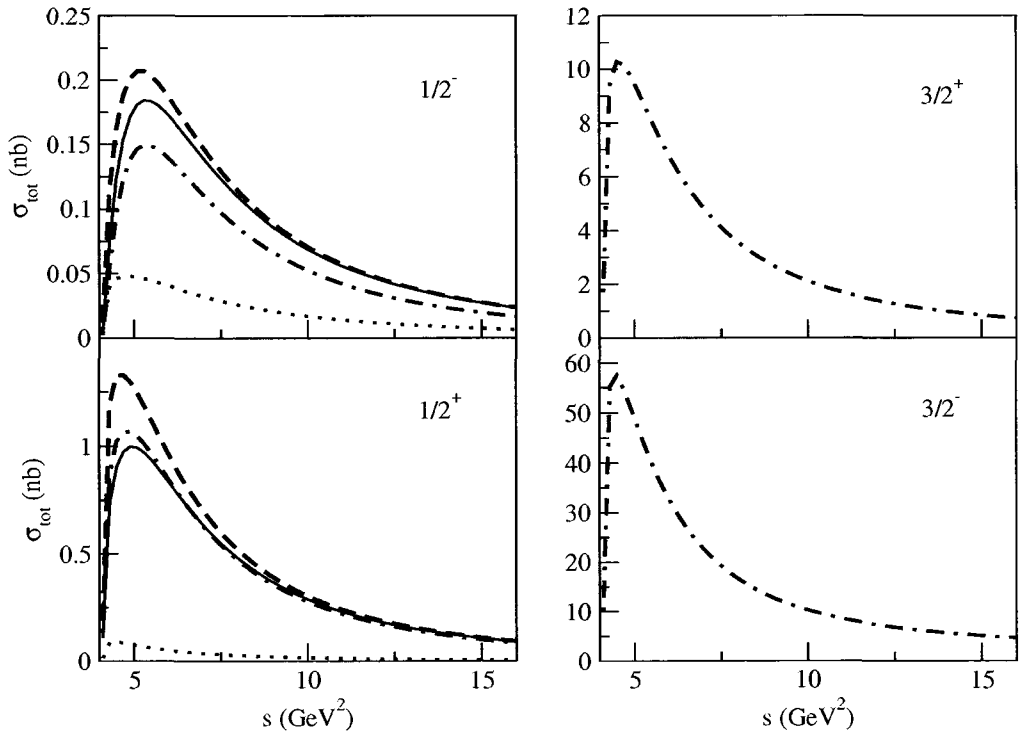

FIG. 5.3: Regge model predictions for the $\gamma n \to K^- \Theta^+$ total cross sections for different spin-parity assignments of the Θ^+ resonance. Curve conventions as in Fig. 5.2.

process gauge-invariant. They are also responsible for the pronounced peak structure in the differential cross section at low values of $-t$. For the cases of $J^P_\Theta = 3/2^\pm$, the situation is reversed, as the $KN\Theta$ coupling constant is about a factor 7 larger for the case of $3/2^-$ compared with the case of $3/2^+$ when using a same width for the Θ^+. Taking into account the u-channel and contact diagrams then yields cross sections for the case of $3/2^-$ which are about a factor of 4 larger than for the case of $3/2^+$.

In Fig. 5.2, we also show our estimates for the K^* exchange process for the spin-parity assignments $1/2^\pm$. To show the range of uncertainty arising from the $K^*N\Theta$ coupling, we display our results for two values : $f_{K^*N\Theta} = +1.1$ and $f_{K^*N\Theta} = -1.1$. The value $f_{K^*N\Theta} = +1.1$ is obtained by rescaling the chiral quark soliton model coupling for the case $J^P_\Theta = 1/2^+$ by the same amount as when rescaling the model value of $g_{KN\Theta}$ to correspond to a width of 1 MeV. One notices from Fig. 5.2 that for a $K^*N\Theta$ coupling

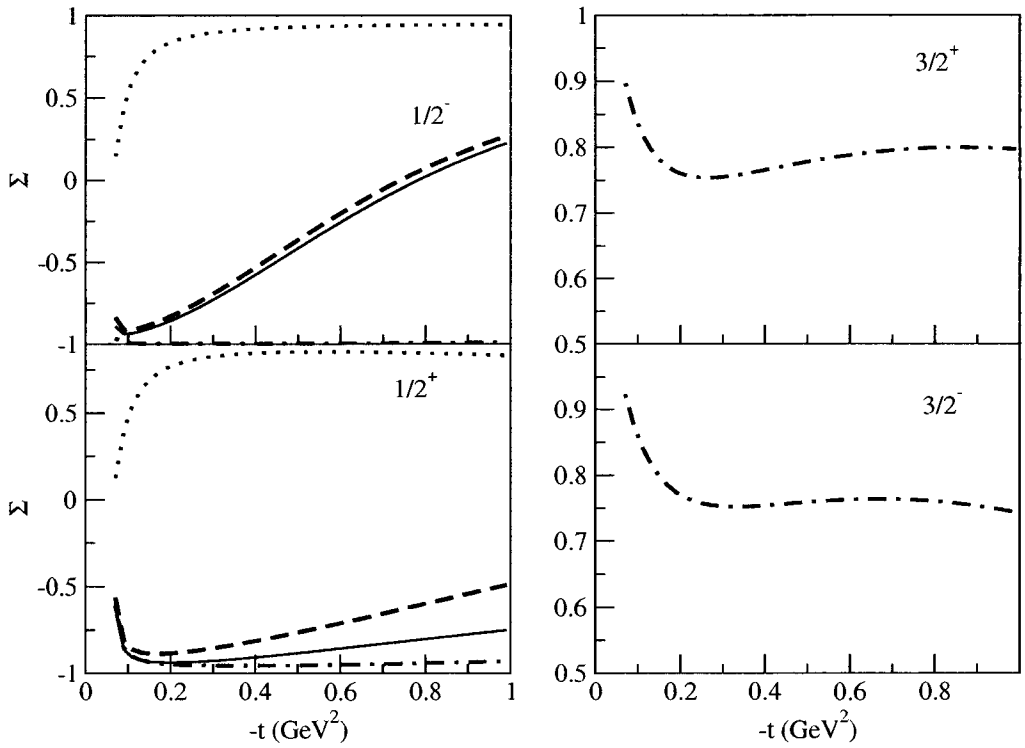

FIG. 5.4: Regge model predictions for the $\gamma n \to K^- \Theta^+$ photon asymmetry at $E_\gamma = 4$ GeV for different spin parity assignments of the Θ^+. Curve conventions as in Fig. 5.2.

within this range, the resulting K^* Regge exchange process yields only a very small contribution to the cross section compared with the gauge-invariant K exchange, in particular for the case of $1/2^+$. Furthermore, in the forward direction the K^* exchange process vanishes due to the momentum $(q - p_K)$ dependence in the $\gamma K K^*$ vertex. Such a behavior has been confirmed by data for the $\gamma p \to K^+ \Sigma^0$ reaction which is dominated by K^* exchange at large s and small $-t$, see Ref. [113]. Analogously, the forward angular region ($-t << s$) for the $\gamma n \to K^- \Theta^+$ reaction at high photon energy is dominated by charged K exchange. At larger values of $-t$ the relative weight of K^* versus K exchange increases. Using the same values for the $K^* N \Theta$ coupling in case $J^P_\Theta = 1/2^-$, the K^* exchange contribution becomes comparable to the gauge-invariant K exchange for values around $-t \simeq 1$ GeV^2.

In Fig. 5.3, we show the corresponding total cross sections. Using a width of 1 MeV

for the Θ^+, the maximum value of the total cross sections can be seen to be around 1 nb for the case of $1/2^+$ and 0.2 nb for the case of $1/2^-$. For the cases of $3/2^+$ $(3/2^-)$ much larger cross sections of around 10 nb (55 nb) are obtained when using a same value of 1 MeV for the Θ^+ width.

A direct measure of the relative weight of K versus K^* exchange processes can be obtained by the linear photon asymmetry, defined as :

$$\Sigma = \frac{\sigma_\perp - \sigma_\parallel}{\sigma_\perp + \sigma_\parallel}, \tag{5.33}$$

where $\sigma_\parallel$ and $\sigma_\perp$ are the cross sections induced by a linearly polarized photon beam with polarization vector lying in the reaction plane (for $\sigma_\parallel$) and perpendicular to the reaction plane (for $\sigma_\perp$) respectively. At high s and small $-t$ (with $-t << s$) the photon asymmetry for a natural parity t-channel exchange (such as for the K^*) approaches the value +1 (i.e. $\sigma_\perp$ dominates), whereas the photon asymmetry for an unnatural parity t-channel exchange process (such as for the K) yields the value -1 (i.e. $\sigma_\parallel$ dominates). The u-channel process and contact diagram, which are needed to make the t-channel K exchange gauge invariant are responsible for the deviation of the photon asymmetry from the value of -1, as is seen on Fig. 5.4. As the $\gamma n \rightarrow K^- \Theta^+$ process at large s and low $-t$ is dominated by K exchange, one sees from Fig. 5.4 that the photon asymmetry rises sharply, at small $-t$, to a large negative value for the cases of $1/2^\pm$. At larger values of $-t$ (for $-t \geq 0.2$ GeV^2), one sees from Fig. 5.4 that the influence of the K^* exchange in the photon asymmetry shows up, in particular for the case of $1/2^-$. The photon asymmetry seems therefore to be a very promising signature to distinguish between the $J^P_\Theta = 1/2^+$ and $J^P_\Theta = 1/2^-$ cases.

In Fig. 5.5, we show the corresponding observables for the $\gamma p \rightarrow \bar{K}^0 \Theta^+$. For the neutral kaon production reaction, the t-channel K exchange is absent, and the dominant t-channel mechanism is K^* exchange. One therefore sees from Figs. 5.5,5.7 that the observables carry the signatures of a K^* dominated process, i.e. a differential cross section which vanishes in the low t region and a photon asymmetry which reaches large positive

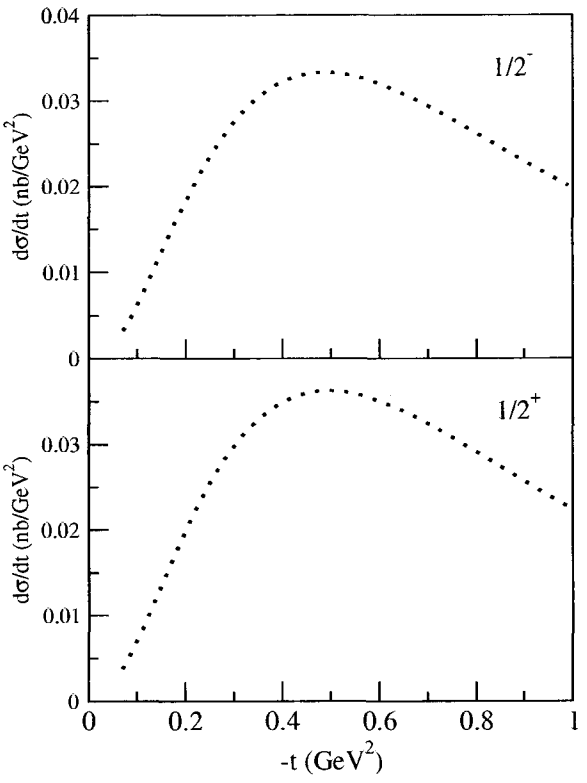

FIG. 5.5: Regge model predictions for the $\gamma p \to \bar{K}^0\Theta^+$ cross section at $E_\gamma = 4$ GeV for different spin-parity assignments of the Θ^+. Dotted curves : K^* Regge exchange.

values. By comparing the processes on the neutron (in Fig. 5.3) and on the proton (in Fig. 5.6), one notices that the absence of the K exchange mechanism yields cross sections on the proton that are about a factor 5 to 10 smaller than their counterparts on the neutron for the cases of $J^P_\Theta = 1/2^\pm$.

We next study the sensitivity of single target or recoil polarization observables for the $\gamma n \to K^-\Theta^+$ reaction, to the spin-parity assignments $J^P_\Theta = 1/2^+$ and $J^P_\Theta = 1/2^-$. The single target spin asymmetry (T) is defined as :

$$T = \frac{\sigma_{\Uparrow} - \sigma_{\Downarrow}}{\sigma_{\Uparrow} + \sigma_{\Downarrow}}, \tag{5.34}$$

where $\sigma_{\Uparrow}$ ($\sigma_{\Downarrow}$) are the cross sections where the target spin is polarized along (opposite) to the vector $\hat{n} \equiv (\vec{q}\times\vec{p}_K)/|\vec{q}\times\vec{p}_K|$, normal to the reaction plane. The recoil spin asymmetry

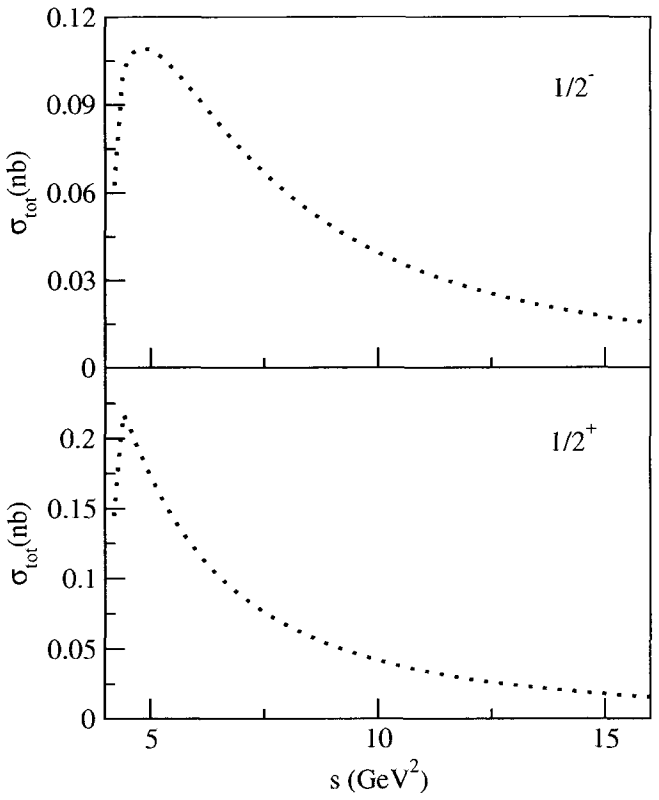

FIG. 5.6: Regge model predictions for the $\gamma p \to \bar{K}^0\Theta^+$ total cross sections for different spin-parity assignments of the Θ^+ resonance. Dotted curves : K^* Regge exchange.

(P) is defined in an analogous way, where the Θ^+ has its spin polarized along or opposite to the normal vector $\hat{n}$. In Figs. 5.8 and 5.9, we compare the Regge model results for T and P for both Θ^+ spin-parity assignments $1/2^{\pm}$. We first notice that the observables T and P are proportional to an imaginary part of the interference of two amplitudes. Therefore, one only obtains a non-zero value for T or P when the two interfering amplitudes exhibit a phase difference. The K exchange or the K^* exchange processes by themselves give us therefore a zero value for the asymmetries T and P. Their sum however leads to a non-zero value for T and P as shown in Figs. 5.8 and 5.9, due to the phase difference between the K and K^* Regge amplitudes. We see from Figs. 5.8 and 5.9 that for $J^P_\Theta = 1/2^+$, T and P have an opposite sign. On the other hand for the situation $J^P_\Theta = 1/2^-$, T and P

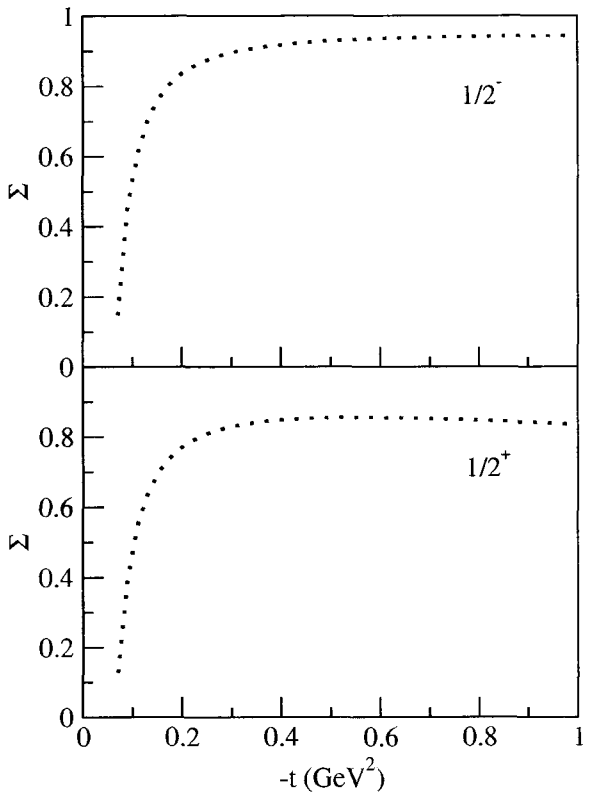

FIG. 5.7: Regge model predictions for the $\gamma p \to \bar{K}^0\Theta^+$ photon asymmetry at $E_\gamma = 4$ GeV for different spin-parity assignments of the Θ^+. Dotted curves : K^* Regge exchange.

display the same sign.

Besides the observables discussed above, where one integrates over all possible final states for the Θ^+ decay, one can also observe the decay angular distributions of the Θ^+. They show a characteristic dependence on the spin and parity of the final state. In the appendix, we list the Θ^+ decay angular distributions for the spin-parity assignments $1/2^\pm$ and $3/2^\pm$.

We show the decay angular distributions for different photon polarizations : unpolarized (0) (Fig. 5.10), linearly polarized in the reaction plane (x) (Fig. 5.11), linearly polarized perpendicular to the reaction plane (y) (Fig. 5.12), and left-handed circular polarization (c, left) (Figs. 5.13 and 5.14). For the spin-parity assignments of $1/2^\pm$, one

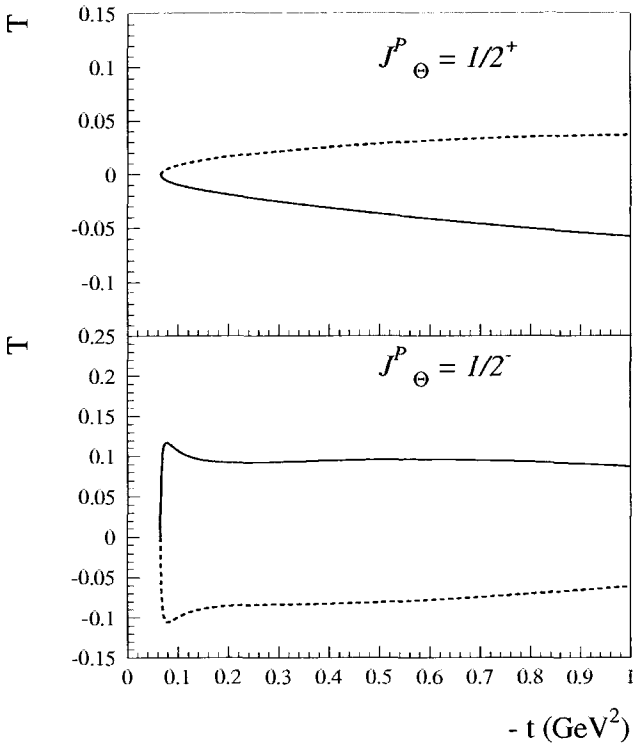

FIG. 5.8: Regge model predictions for the target single spin asymmetry T for the $\gamma n \to K^- \Theta^+$ reaction for both possible parities of the Θ^+ resonance (for $J = 1/2$) at $E_\gamma = 4$ GeV. The model calculations correspond with the $K + K^*$ Regge exchanges for two values of the $K^* N \Theta$ coupling. Solid curves : $f_{K^* N \Theta} = +1.1$, dashed curves : $f_{K^* N \Theta} = -1.1$.

notices that the decay angular distributions (0), (x) and (y) display a nearly flat angular dependence. The decay angular distribution for a circularly polarized photon (c, left) on the other hand, is flat for the case of $1/2^-$ but not uniform for $1/2^+$, allowing to distinguish between both parity cases. All decay angular distributions show characteristic angular dependences in the case of $3/2^\pm$, which would be easily distinguishable from the $1/2^\pm$ case.

In Fig. 5.15, we also show our results for the $\gamma p \to \bar{K}^{*0} \Theta^+$ reaction. For this process, the dominant t-channel exchange mechanism, at high s and low $-t$, is given by K^0 exchange as shown in Fig. 5.1 (lower right panel). This yields to strong forwardly

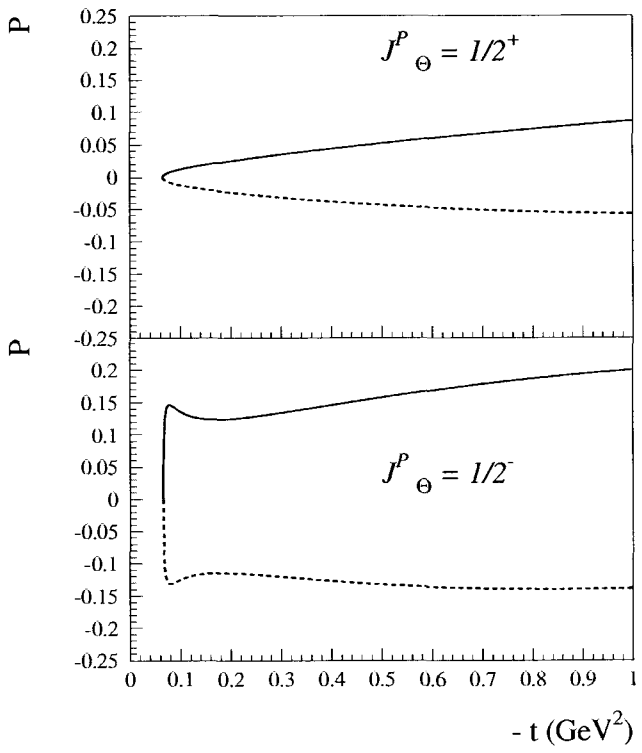

FIG. 5.9: Regge model predictions for the recoil single spin asymmetry P for the $\gamma n \to K^{*-}\Theta^+$ reaction for both possible parities of the Θ^+ resonance (for $J = 1/2$) at $E_\gamma = 4$ GeV. Curve conventions as in Fig. 5.8.

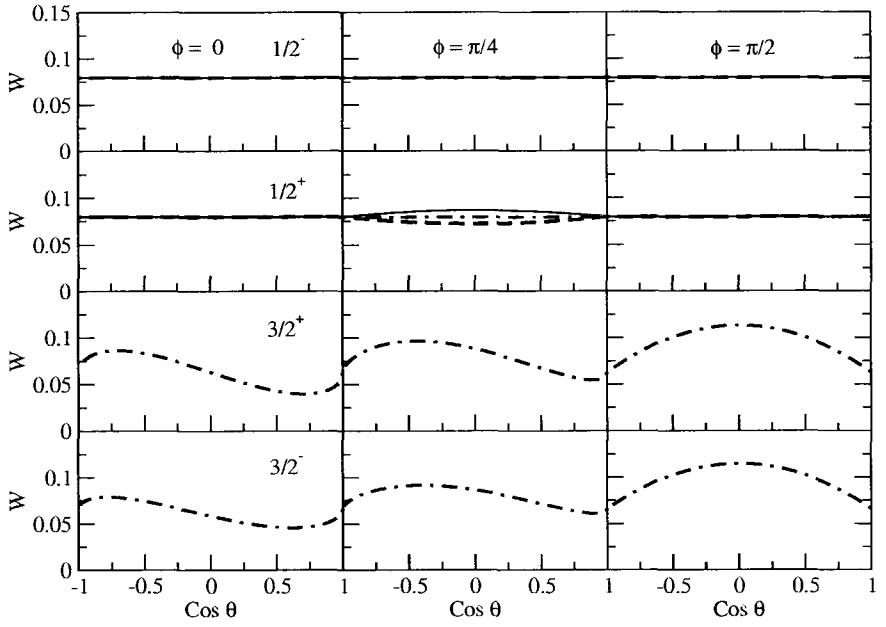

FIG. 5.10: Regge model predictions for the $\gamma n \to K^- \Theta^+$ angular distribution for an unpolarized photon (0) for different spin parity assignments of the Θ^+, and for different decay angles (θ, ϕ), defi ned in the rest frame of the Θ^+. Dashed-dotted curves : K Regge exchange; dotted curves : K^* Regge exchange; solid curves : $K + K^*$ Regge exchanges.

peaked angular distributions, as is seen from Fig. 5.15. For a Θ^+ width of 1 MeV, the $1/2^+$ $(1/2^-)$ total cross sections reach a maximum value of 1.2 nb (0.2 nb) respectively.

5.4 Conclusions

In this work, we studied the reaction mechanism for the photoproduction of the $\Theta^+(1540)$ resonance on the nucleon, through K and K^* Regge exchanges. Our estimates depend on only two parameters : the $KN\Theta^+$ and $K^*N\Theta^+$ coupling constants. The $KN\Theta^+$ coupling constant is directly related to the Θ^+ width. We determine the $K^*N\Theta^+$ coupling constant by rescaling the value obtained from the chiral quark soliton model by the same amount one has to rescale the $KN\Theta^+$ coupling to yield a given value of the Θ^+ width.

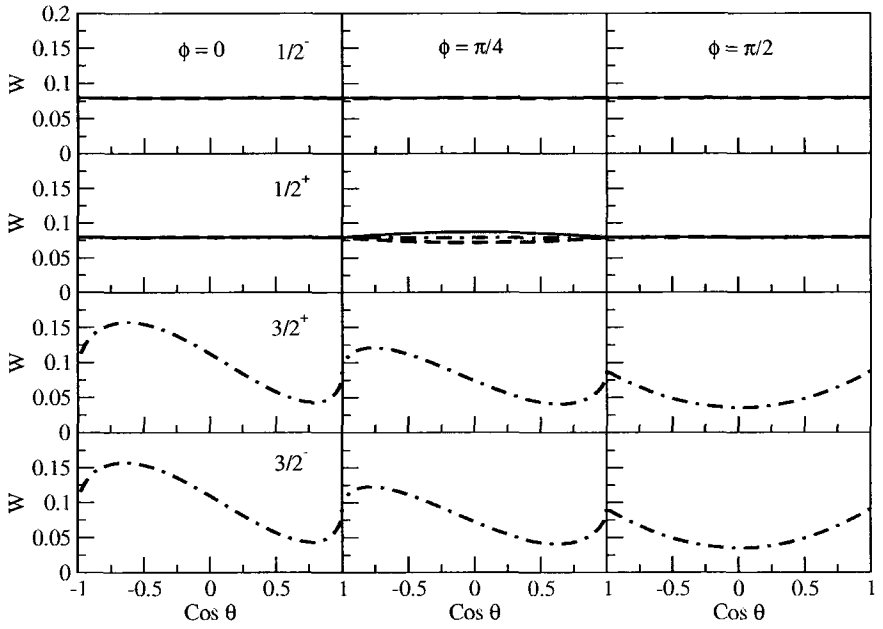

FIG. 5.11: Regge model predictions for the $\gamma n \rightarrow K^{-}\Theta^{+}$ angular distribution for a photon linearly polarized in the reaction plane (x) for different spin parity assignments of the Θ^{+}. Curve conventions as in Fig. 5.10.

In the Regge model, which is assumed to be valid above *c.m.* energies above 2 GeV, the Θ^{+} photoproduction cross sections show a strong forward angular dependence. We compared the size of the cross sections for the $\gamma n \rightarrow K^{-}\Theta^{+}$ and $\gamma p \rightarrow \bar{K}^{0}\Theta^{+}$ reactions, and investigate their sensitivity to the spin-parity assignments $J^{P} = \frac{1}{2}^{\pm}, \frac{3}{2}^{\pm}$ for the Θ^{+} resonance. Using the Regge model, we estimated the cross sections corresponding with a given upper bound on the width of the Θ^{+}. Within this model, the cross sections on the neutron were found to be around a factor 5 larger than the ones on the proton, due to the presence of charged K exchange for the reaction on a neutron target. For the case of spin-parity $J^{P} = \frac{1}{2}^{+}$, we found that a Θ^{+} width of 1 MeV yields $\gamma n \rightarrow K^{-}\Theta^{+}$ cross sections of around 1 nb, and $\gamma p \rightarrow \bar{K}^{0}\Theta^{+}$ cross sections around 0.2 nb. In the absence of a signal of the Θ^{+} in such reactions, our estimates may be used to translate a given cross section upper limit into an upper bound on the width of the Θ^{+}.

Furthermore, we also estimated the photon asymmetry which was found to display

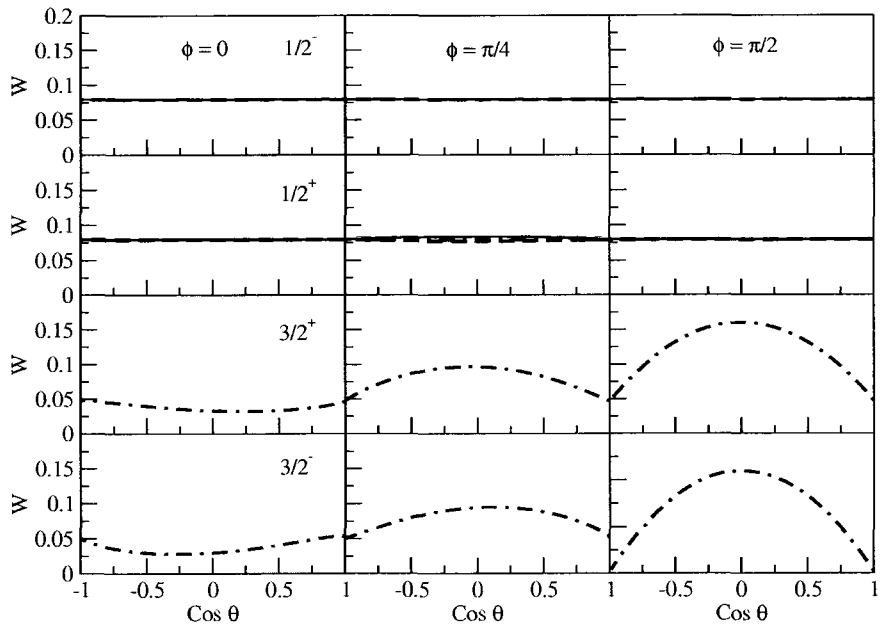

FIG. 5.12: Regge model predictions for the $\gamma n \rightarrow K^{-}\Theta^{+}$ angular distribution for a photon linearly polarized perpendicular to the reaction plane (y) for different spin parity assignments of the Θ^{+}. Curve conventions as in Fig. 5.10.

a pronounced sensitivity to the parity of the Θ^{+}. Provided the Θ^{+} can be produced, the photon asymmetry would be a very promising observable to help determining the quantum numbers of the Θ^{+} resonance.

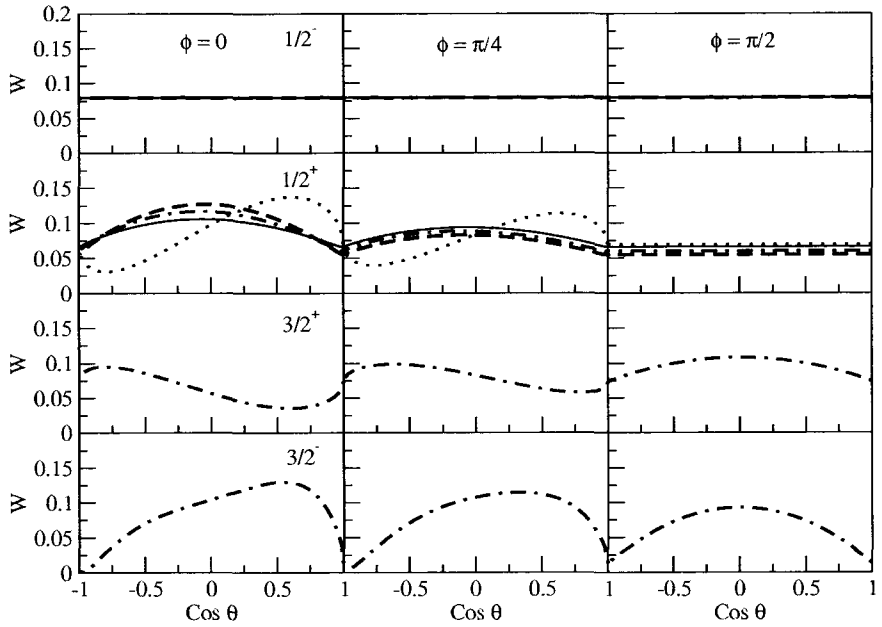

FIG. 5.13: Regge model predictions for the $\gamma n \to K^- \Theta^+$ angular distribution for a left-handed circularly polarized photon (c, left) for different spin parity assignments of the Θ^+. Curve conventions as in Fig. 5.10.

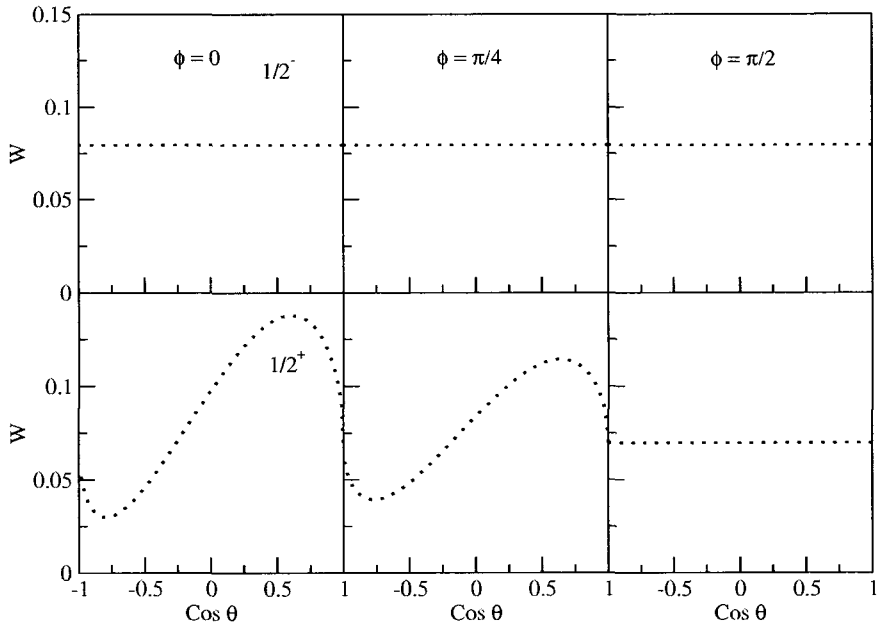

FIG. 5.14: Regge model predictions for the $\gamma p \to K^{*0}\Theta^{+}$ angular distribution (c, left) for different spin parity assignments of the Θ^{+}. Dotted curves : K^{*} Regge exchange.

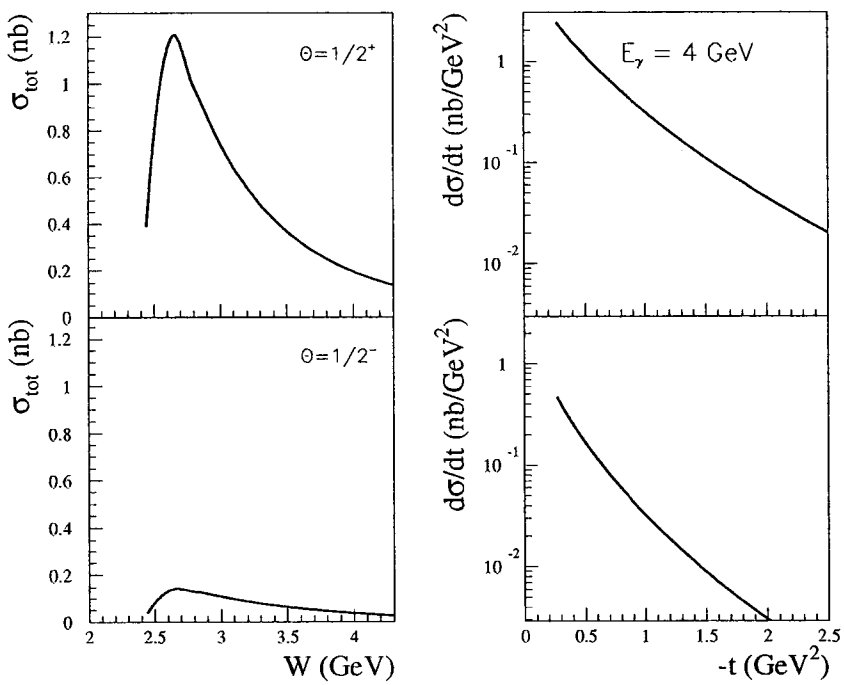

FIG. 5.15: Regge model predictions for the $\gamma p \to \bar{K}^{*0}\Theta^+$ reaction for both possible parities of the Θ^+ resonance. Upper panels : positive parity case; lower panels : negative parity case. Left panels : total cross section; right panels : differential cross section at $E_\gamma = 4$ GeV. The model calculation corresponds with K^0 Regge exchange.

APPENDIX A

Decay Angular Distribution

After produced, the Θ^+ decays into $\bar{K}^0 p$ or $K^+ n$ in 50% ratio. The angular distribution of the decay product (Kaon) can be determined by:

$$\begin{aligned} W(\theta,\phi) &= \sum_{s_f,s'_f;s_\theta,s'_\theta} \hat{R}_{s_f,s_\theta}\rho_{s_\theta,s'_\theta}(\Theta^+)\hat{R}^*_{s'_f,s'_\theta} \\ &= \sum_{s_\theta,s'_\theta} \left\{ \hat{R}_{-\frac{1}{2},s_\theta}\rho_{s_\theta,s'_\theta}\hat{R}^*_{-\frac{1}{2},s'_\theta} + \hat{R}_{\frac{1}{2},s_\theta}\rho_{s_\theta,s'_\theta}\hat{R}^*_{-\frac{1}{2},s'_\theta} \right. \\ &\quad \left. + \hat{R}_{\frac{1}{2},s_\theta}\rho_{s_\theta,s'_\theta}\hat{R}^*_{\frac{1}{2},s'_\theta} + \hat{R}_{-\frac{1}{2},s_\theta}\rho_{s_\theta,s'_\theta}\hat{R}^*_{\frac{1}{2},s'_\theta} \right\}, \end{aligned} \tag{A.1}$$

where the transition operator $\hat{R}_{s_f,s_\theta}$ is defined as follow:

$$\hat{R}_{s_f,s_\theta} \equiv \langle N, s_f, \mathbf{P}_\theta - \mathbf{p}'|\hat{t}|\Theta^+, s_\theta, \mathbf{P}_\theta = 0\rangle, \tag{A.2}$$

and the photon density matrix elements $\rho_{s_\theta,s'_\theta}$ in the Θ^+ production can be obtained by squaring the amplitude $\mathcal{M}_K$ $(\gamma N \rightarrow \Theta^+ K)$ of the corresponding spin of the Θ^+ and summing over the spin of the nucleon and the helicity of the photon.

The transition operator $\hat{R}_{s_f,s_\theta}$ depends on the spin of the particles involved. Below is the list of the transition operator $\hat{R}_{s_f,s_\theta}$ we use in this paper:

- $J^P = \frac{1}{2}^-$

$$\hat{R}_{s_f,s_\theta} = \mathcal{C}\delta_{s_f,s_\theta}$$

- $J^P = \frac{1}{2}^+$

$$\begin{aligned}
\hat{R}_{\frac{1}{2},\frac{1}{2}} &= \cos\theta \\
\hat{R}_{\frac{1}{2},-\frac{1}{2}} &= -\sin\theta\ e^{-i\phi} \\
\hat{R}_{-\frac{1}{2},\frac{1}{2}} &= -\sin\theta\ e^{i\phi} \\
\hat{R}_{-\frac{1}{2},-\frac{1}{2}} &= -\cos\theta
\end{aligned}$$

- $J^P = \frac{3}{2}^+$

$$\begin{aligned}
\hat{R}_{\frac{1}{2},\frac{3}{2}} &= \frac{\sin\theta}{\sqrt{2}}\ e^{i\phi} \\
\hat{R}_{\frac{1}{2},\frac{1}{2}} &= \sqrt{\frac{2}{3}}\cos\theta \\
\hat{R}_{\frac{1}{2},-\frac{1}{2}} &= -\sqrt{\frac{1}{6}}\sin\theta\ e^{-i\phi} \\
\hat{R}_{-\frac{1}{2},\frac{1}{2}} &= \sqrt{\frac{1}{6}}\sin\theta\ e^{i\phi} \\
\hat{R}_{-\frac{1}{2},-\frac{1}{2}} &= \sqrt{\frac{2}{3}}\cos\theta \\
\hat{R}_{-\frac{1}{2},-\frac{3}{2}} &= -\frac{\sin\theta}{\sqrt{2}}\ e^{i\phi}
\end{aligned}$$

- $J^P = \frac{3}{2}^-$

$$
\begin{aligned}
\hat{R}_{\frac{1}{2},\frac{3}{2}} &= -\sqrt{\frac{3}{40}}\sin 2\theta\ e^{i\phi} \\
\hat{R}_{\frac{1}{2},\frac{1}{2}} &= -\sqrt{\frac{1}{10}}(3\cos^2\theta - 1) \\
\hat{R}_{\frac{1}{2},-\frac{1}{2}} &= \sqrt{\frac{9}{40}}\sin 2\theta\ e^{-i\phi} \\
\hat{R}_{\frac{1}{2},-\frac{3}{2}} &= -\sqrt{\frac{3}{10}}\sin^2\theta\ e^{-2i\phi} \\
\hat{R}_{-\frac{1}{2},\frac{3}{2}} &= \sqrt{\frac{3}{10}}\sin^2\theta\ e^{2i\phi} \\
\hat{R}_{-\frac{1}{2},\frac{1}{2}} &= \sqrt{\frac{9}{40}}\sin 2\theta\ e^{i\phi} \\
\hat{R}_{-\frac{1}{2},-\frac{1}{2}} &= \sqrt{\frac{1}{10}}(3\cos^2\theta - 1) \\
\hat{R}_{-\frac{1}{2},-\frac{3}{2}} &= -\sqrt{\frac{3}{40}}\sin 2\theta\ e^{-i\phi}
\end{aligned}
$$

BIBLIOGRAPHY

[1] T. Nakano et al. (LEPS), Phys. Rev. Lett. **91**, 012002 (2003), hep-ex/0301020.

[2] S. Stepanyan et al. (CLAS), Phys. Rev. Lett. **91**, 252001 (2003), hep-ex/0307018.

[3] J. Barth et al. (SAPHIR), Phys. Lett. **B572**, 127 (2003), hep-ex/0307083.

[4] V. Kubarovsky and S. Stepanyan (CLAS), AIP Conf. Proc. **698**, 543 (2004), hep-ex/0307088.

[5] V. V. Barmin et al. (DIANA), Phys. Atom. Nucl. **66**, 1715 (2003), hep-ex/0304040.

[6] M. Abdel-Bary et al. (COSY-TOF), Phys. Lett. **B595**, 127 (2004), hep-ex/0403011.

[7] A. Airapetian et al. (HERMES), Phys. Lett. **B585**, 213 (2004), hep-ex/0312044.

[8] S. Chekanov et al. (ZEUS), Phys. Lett. **B591**, 7 (2004), hep-ex/0403051.

[9] A. Aleev et al. (SVD) (2004), hep-ex/0401024.

[10] A. E. Asratyan, A. G. Dolgolenko, and M. A. Kubantsev, Phys. Atom. Nucl. **67**, 682 (2004), hep-ex/0309042.

[11] K. H. Hicks (2005), hep-ex/0504027.

[12] A. R. Dzierba, D. Krop, M. Swat, S. Teige, and A. P. Szczepaniak, Phys. Rev. **D69**, 051901 (2004), hep-ph/0311125.

[13] K. Hicks, V. Burkert, A. E. Kudryavtsev, I. I. Strakovsky, and S. Stepanyan (2004), hep-ph/0411265.

[14] *JLab Hall B experiment E-04-021, spokespersons* M. Battaglieri, Raffaella De Vita, Thomas Jefferson National Accelerator Facility, Newport News, Virginia (2004).

[15] S.-I. Nam, A. Hosaka, and H.-C. Kim (2004), hep-ph/0403009.

[16] W. Liu and C. M. Ko, Phys. Rev. **C68**, 045203 (2003), nucl-th/0308034.

[17] W. Liu and C. M. Ko, Nucl. Phys. **A741**, 215 (2004), nucl-th/0309023.

[18] H. Kwee, M. Guidal, M. V. Polyakov, and M. Vanderhaeghen (2005), hep-ph/0507180.

[19] K.-T. Brinkmann, *Search for the Pentaquark(s), Talk Given at CAP 2005, Vancouver, Canada* (2005).

[20] J. Z. Bai et al. (BES), Phys. Rev. **D70**, 012004 (2004), hep-ex/0402012.

[21] B. Aubert et al. (BABAR) (2004), hep-ex/0408064.

[22] K. Abe et al. (BELLE) (2004), hep-ex/0409010.

[23] S. Schael et al. (ALEPH), Phys. Lett. **B599**, 1 (2004).

[24] I. Abt et al. (HERA-B), Phys. Rev. Lett. **93**, 212003 (2004), hep-ex/0408048.

[25] Y. M. Antipov et al. (SPHINX), Eur. Phys. J. **A21**, 455 (2004), hep-ex/0407026.

[26] M. J. Longo et al. (HyperCP), Phys. Rev. **D70**, 111101 (2004), hep-ex/0410027.

[27] D. O. Litvintsev (CDF), Nucl. Phys. Proc. Suppl. **142**, 374 (2005), hep-ex/0410024.

[28] K. Stenson (FOCUS) (2004), hep-ex/0412021.

[29] K. Abe et al. (Belle) (2004), hep-ex/0411005.

[30] C. Pinkenburg (PHENIX), J. Phys. **G30**, S1201 (2004), nucl-ex/0404001.

[31] F. Stancu and D. O. Riska, Phys. Lett. **B575**, 242 (2003), hep-ph/0307010.

[32] H. Hogaasen and P. Sorba, Nucl. Phys. **B145**, 119 (1978).

[33] M. de Crombrugghe, H. Hogaasen, and P. Sorba, Nucl. Phys. **B156**, 347 (1979).

[34] D. Strottman, Phys. Rev. **D20**, 748 (1979).

[35] C. Roiesnel, Phys. Rev. **D20**, 1646 (1979).

[36] H. J. Lipkin, Phys. Lett. **B195**, 484 (1987).

[37] C. Gignoux, B. Silvestre-Brac, and J. M. Richard, Phys. Lett. **B193**, 323 (1987).

[38] J. Leandri and B. Silvestre-Brac, Phys. Rev. **D40**, 2340 (1989).

[39] S. Capstick, P. R. Page, and W. Roberts, Phys. Lett. **B570**, 185 (2003), hep-ph/0307019.

[40] B. G. Wybourne (2003), hep-ph/0307170.

[41] M. Karliner and H. J. Lipkin (2003), hep-ph/0307243.

[42] A. Hosaka, Phys. Lett. **B571**, 55 (2003), hep-ph/0307232.

[43] R. L. Jaffe and F. Wilczek, Phys. Rev. Lett. **91**, 232003 (2003), hep-ph/0307341.

[44] H. Walliser and V. B. Kopeliovich, J. Exp. Theor. Phys. **97**, 433 (2003), hep-ph/0304058.

[45] S.-L. Zhu, Phys. Rev. Lett. **91**, 232002 (2003), hep-ph/0307345.

[46] N. G. Kelkar, M. Nowakowski, and K. P. Khemchandani, J. Phys. **G29**, 1001 (2003), hep-ph/0307134.

[47] S. Nussinov (2003), hep-ph/0307357.

[48] D. Borisyuk, M. Faber, and A. Kobushkin (2003), hep-ph/0307370.

[49] Y.-s. Oh, B.-Y. Park, and D.-P. Min, Phys. Lett. **B331**, 362 (1994), hep-ph/9405297.

[50] D. O. Riska and N. N. Scoccola, Phys. Lett. **B299**, 338 (1993).

[51] D. Diakonov, V. Petrov, and M. V. Polyakov, Z. Phys. **A359**, 305 (1997), hep-ph/9703373.

[52] R. L. Jaffe, Phys. Rev. **D15**, 281 (1977).

[53] C. E. Carlson, C. D. Carone, H. J. Kwee, and V. Nazaryan, Phys. Lett. **B579**, 52 (2004), hep-ph/0310038.

[54] A. Chodos, R. L. Jaffe, K. Johnson, C. B. Thorn, and V. F. Weisskopf, Phys. Rev. **D9**, 3471 (1974).

[55] T. DeGrand, R. L. Jaffe, K. Johnson, and J. E. Kiskis, Phys. Rev. **D12**, 2060 (1975).

[56] C. E. Carlson, T. H. Hansson, and C. Peterson, Phys. Rev. **D27**, 1556 (1983).

[57] M. S. Chanowitz and S. R. Sharpe, Nucl. Phys. **B222**, 211 (1983).

[58] L. Y. Glozman and D. O. Riska, Phys. Rept. **268**, 263 (1996), hep-ph/9505422.

[59] C. D. Carone, H. Georgi, L. Kaplan, and D. Morin, Phys. Rev. **D50**, 5793 (1994), hep-ph/9406227.

[60] M. Chemtob, Nucl. Phys. **B256**, 600 (1985).

[61] H. Weigel, Eur. Phys. J. **A2**, 391 (1998), hep-ph/9804260.

[62] T. D. Cohen, Phys. Lett. **B581**, 175 (2004), hep-ph/0309111.

[63] R. W. Gothe and S. Nussinov (2003), hep-ph/0308230.

[64] K. Cheung, Phys. Rev. **D69**, 094029 (2004), hep-ph/0308176.

[65] C. E. Carlson, C. D. Carone, H. J. Kwee, and V. Nazaryan, Phys. Lett. **B573**, 101 (2003), hep-ph/0307396.

[66] B. K. Jennings and K. Maltman, Phys. Rev. **D69**, 094020 (2004), hep-ph/0308286.

[67] M. Praszalowicz, Phys. Lett. **B575**, 234 (2003), hep-ph/0308114.

[68] J. Randrup, Phys. Rev. **C68**, 031903 (2003), nucl-th/0307042.

[69] T. Hyodo, A. Hosaka, and E. Oset, Phys. Lett. **B579**, 290 (2004), nucl-th/0307105.

[70] L. W. Chen, V. Greco, C. M. Ko, S. H. Lee, and W. Liu, Phys. Lett. **B601**, 34 (2004), nucl-th/0308006.

[71] Y.-s. Oh, H.-c. Kim, and S. H. Lee, Phys. Rev. **D69**, 014009 (2004), hep-ph/0310019.

[72] R. A. Arndt, I. I. Strakovsky, and R. L. Workman, Phys. Rev. **C68**, 042201 (2003), nucl-th/0308012.

[73] J. Haidenbauer and G. Krein, Phys. Rev. **C68**, 052201 (2003), hep-ph/0309243.

[74] T. D. Cohen and R. F. Lebed, Phys. Lett. **B578**, 150 (2004), hep-ph/0309150.

[75] P. Bicudo and G. M. Marques, Phys. Rev. **D69**, 011503 (2004), hep-ph/0308073.

[76] R. D. Matheus, F. S. Navarra, M. Nielsen, R. Rodrigues da Silva, and S. H. Lee, Phys. Lett. **B578**, 323 (2004), hep-ph/0309001.

[77] F. Csikor, Z. Fodor, S. D. Katz, and T. G. Kovacs, JHEP **11**, 070 (2003), hep-lat/0309090.

[78] J. Sugiyama, T. Doi, and M. Oka, Phys. Lett. **B581**, 167 (2004), hep-ph/0309271.

[79] L. Y. Glozman, Phys. Lett. **B575**, 18 (2003), hep-ph/0308232.

[80] N. Isgur and G. Karl, Phys. Rev. **D18**, 4187 (1978).

[81] C. E. Carlson, C. D. Carone, J. L. Goity, and R. F. Lebed, Phys. Lett. **B438**, 327 (1998), hep-ph/9807334.

[82] C. E. Carlson, C. D. Carone, J. L. Goity, and R. F. Lebed, Phys. Rev. **D59**, 114008 (1999), hep-ph/9812440.

[83] H. Collins and H. Georgi, Phys. Rev. **D59**, 094010 (1999), hep-ph/9810392.

[84] C. L. Schat, J. L. Goity, and N. N. Scoccola, Phys. Rev. Lett. **88**, 102002 (2002), hep-ph/0111082.

[85] J. L. Goity, C. L. Schat, and N. N. Scoccola, Phys. Rev. **D66**, 114014 (2002), hep-ph/0209174.

[86] D. Pirjol and C. Schat, Phys. Rev. **D67**, 096009 (2003), hep-ph/0301187.

[87] F. Myhrer and J. Wroldsen, Phys. Lett. **B139**, 81 (1984).

[88] J. Wroldsen and F. Myhrer, Z. Phys. **C25**, 59 (1984).

[89] F. Myhrer and J. Wroldsen, Z. Phys. **C25**, 281 (1984).

[90] R. F. Dashen, E. Jenkins, and A. V. Manohar, Phys. Rev. **D51**, 3697 (1995), hep-ph/9411234.

[91] C. Alt et al. (NA49), Phys. Rev. Lett. **92**, 042003 (2004), hep-ex/0310014.

[92] D. Borisyuk, M. Faber, and A. Kobushkin, Ukr. J. Phys. **49**, 944 (2004), hep-ph/0312213.

[93] J. J. Dudek and F. E. Close, Phys. Lett. **B583**, 278 (2004), hep-ph/0311258.

[94] F. Stancu, Phys. Rev. **D58**, 111501 (1998), hep-ph/9803442.

[95] Y.-s. Oh, H. c. Kim, and S. H. Lee, Phys. Rev. **D69**, 094009 (2004), hep-ph/0310117.

[96] Y.-s. Oh, H. Kim, and S. H. Lee, Phys. Rev. **D69**, 074016 (2004), hep-ph/0311054.

[97] Y.-s. Oh, H.-c. Kim, and S. H. Lee, Nucl. Phys. **A745**, 129 (2004), hep-ph/0312229.

[98] A. Manohar and H. Georgi, Nucl. Phys. **B234**, 189 (1984).

[99] M. Aguilar-Benitez et al., Phys. Lett. **B170**, 1 (1986).

[100] C. E. Carlson, C. D. Carone, H. J. Kwee, and V. Nazaryan, Phys. Rev. **D70**, 037501 (2004), hep-ph/0312325.

[101] S. I. Nam, A. Hosaka, and H. C. Kim, Phys. Lett. **B579**, 43 (2004), hep-ph/0308313.

[102] S. I. Nam, A. Hosaka, and H. C. Kim, Phys. Rev. **D70**, 114027 (2004), hep-ph/0402138.

[103] Q. Zhao, Phys. Rev. **D69**, 053009 (2004), hep-ph/0310350.

[104] K. Nakayama and K. Tsushima, Phys. Lett. **B583**, 269 (2004), hep-ph/0311112.

[105] Q. Zhao and J. S. Al-Khalili, Phys. Lett. **B585**, 91 (2004), hep-ph/0312348.

[106] F. E. Close and Q. Zhao, Phys. Lett. **B590**, 176 (2004), hep-ph/0403159.

[107] K. Nakayama and W. G. Love, Phys. Rev. **C70**, 012201 (2004), hep-ph/0404011.

[108] T. Mart, Phys. Rev. **C71**, 022202 (2005), nucl-th/0412096.

[109] W. Roberts, Phys. Rev. **C70**, 065201 (2004), nucl-th/0408034.

[110] W. Roberts (2004), nucl-th/0412041.

[111] M. Diehl, B. Pire, and L. Szymanowski, Phys. Lett. **B584**, 58 (2004), hep-ph/0312125.

[112] *JLab Hall B experiment E-03-113, spokespersons* K. Hicks, Stepan Stepanyan, Thomas Jefferson National Accelerator Facility, Newport News, Virginia (2004).

[113] M. Guidal, J. M. Laget, and M. Vanderhaeghen, Nucl. Phys. **A627**, 645 (1997).

[114] M. Guidal, J. M. Laget, and M. Vanderhaeghen, Phys. Rev. **C61**, 025204 (2000), hep-ph/9904511.

[115] M. Guidal, J. M. Laget, and M. Vanderhaeghen, Phys. Rev. **C68**, 058201 (2003), hep-ph/0308131.

[116] *JLab Hall A experiment E-04-012, spokespersons* B. Wojtsekhowski, Thomas Jefferson National Accelerator Facility, Newport News, Virginia (2005).

[117] N. Levy, W. Majerotto, and B. J. Read, Nucl. Phys. **B55**, 493 (1973).

[118] P. Collins, *An Introduction to Regge Theory and High-Energy Physics* (Cambridge University Press, Cambridge, 1977).

[119] R. N. Cahn and G. H. Trilling, Phys. Rev. **D69**, 011501 (2004), hep-ph/0311245.

[120] L. M. Jones, Rev. Mod. Phys. **52**, 545 (1980).

[121] O. Dumbrajs et al., Nucl. Phys. **B216**, 277 (1983).

[122] R. K. G. Hoehler, F. Kaiser and E. Pietarinen, in *Elastic and Charge Exchange Scattering of Elementary Particles–Pion Nucleon Scattering*, edited by H. Schopper (Springer-Verlag, Berlin-Heidelberg-New York, 1983), vol. 9b of *Numerical Data and Functional Relationships in Science and Technology*.

VITA

Herry Kwee

Herry Kwee was born on September 10, 1976 in Palembang, Indonesia. Since his youth he has always been curious about many things related to science and math. He began his formal education in 1983 at St. Xavier V Elementary School in his hometown. In 1989, he entered St. Xavier-Maria Junior High School in the same city. Three years later, in 1992, he entered St. Xavier I High School also in the same city. In the year he graduated from high school, 1995, he participated in the XXVI International Physics Olympiad in Canberra, Australia and won and honorable mention title. In the same year, he started his undergraduate education at Institute Technology of Bandung in Bandung, Indonesia. He chose to major in physics and finished his study in 1999 and graduate with Cumm Laude. After that he took the challenge to continue his study in a country with a different culture. He entered the College of William and Mary in Williamsburg, Virginia in Fall 2000, to study in the physics graduate program. In 2001, he started to work with Dr. Christopher Carone in nuclear particle group. Upon finishing his study there he plans to continue his research in the field of particle physics.